Takala, T.; Lotsari, E.; Polvi, Lina E.

Surface flow and ice rafting velocities during freezing and thawing periods in Nordic rivers

Published in:
Journal of Hydrology

DOI:
10.1016/j.jhydrol.2024.132447

Published: 01/03/2025

Document Version
Publisher's PDF, also known as Version of record

Please cite the original version:
Takala, T., Lotsari, E., & Polvi, L. E. (2025). Surface flow and ice rafting velocities during freezing and thawing periods in Nordic rivers. *Journal of Hydrology*, *649*, Article 132447. https://doi.org/10.1016/j.jhydrol.2024.132447

Journal of Hydrology 649 (2025) 132447

Contents lists available at ScienceDirect

Journal of Hydrology

journal homepage: www.elsevier.com/locate/jhydrol

Surface flow and ice rafting velocities during freezing and thawing periods in Nordic rivers

T. Takala [a,*], E. Lotsari [a,b], L.E. Polvi [c]

[a] Water and Environmental Engineering, Department of Built Environment, Aalto University, P.O. Box 15200, Tietotie 1E, 00076 Aalto, Finland
[b] Department of Geographical and Historical Studies, University of Eastern Finland, Joensuu, Finland
[c] Department of Ecology and Environmental Science, Umeå University, Umeå, Sweden

ARTICLE INFO

This manuscript was handled by Emmanouil Anagnostou, Editor-in-Chief

Keywords:
Surface flow velocity
Frazil ice
River ice
Partial ice cover
Image velocimetry

ABSTRACT

In the present climate, almost all high-latitude rivers in northern regions freeze every winter. In the future, however, climate change may cause shifts in freezing, duration and breakup of river ice cover, runoff, and sediment transport. The main aim of the study is to determine changes in surface flow velocity during river ice freezing and melting periods. We also examine the interplay between surface flow velocity and the initiation and progress of freezing and break-up. The study was performed in three Nordic rivers: the Pulmanki (northern Finland), the Koita (eastern Finland), and the Sävar (northern Sweden). They represent different slope and depth conditions and are representative of boreal and sub-arctic channel types. The flow characteristics were measured and remote sensing data for video-based surface velocimetry analyses (STIV) were collected during one season in each river during autumn ice-formation and spring ice break-up. STIV enabled analyses of surface flow velocities, which were compared to direct flow measurements and against freezing (incl. frazil ice, and partial ice cover) and break-up characteristics.

Notable variations were observed in the interaction between ice cover and flow velocities among the three rivers. The Pulmanki River showed the most rapid decrease in flow velocities during freezing due to increased friction from the ice cover. Continuous frazil ice formation occurred in the Sävar and Pulmanki Rivers, while the Koita River experienced intermittent episodes. Temperature was key in accelerating freezing during colder days and causing ice break-up during warmer days. During the melting period, the Pulmanki River had the highest flow velocities during melting, while the Koita and Sävar Rivers showed a steady increase as the ice melted. Regression models showed that higher flow velocities reduced ice cover, with air temperature also influencing ice behavior. The STIV method enabled effective detection of flow and ice rafting and proved useful for tracking river ice with affordable time-lapse cameras. These findings provide valuable insights for managing river systems in cold climates.

1. Introduction

More than one-third of the Earth's landmass is drained by rivers that freeze seasonally (Yang et al., 2020), and further, nearly 60% of rivers in the northern hemisphere are affected by ice during winter (Prowse, 2005). Climate change not only alters seasonal river discharges (MacDonald et al., 2018) but also affects river ice regimes. A trend of decreasing ice-cover duration is evident in numerous rivers (e.g., Fukś, 2023; Ionita et al., 2018; Magnuson et al., 2000; Norrgård and Helama, 2022; Veijalainen et al., 2010), and it has been projected that river ice cover will continue to diminish globally throughout the 21st century (Yang et al., 2020). The significance of river ice is substantial, as it, along with discharge, regulates key aspects of river systems such as flow dynamics, flood occurrences, and sediment transport (Kämäri et al., 2015; Lotsari et al., 2019; Prowse, 2001). These factors, in turn, have a profound impact on ecosystem function and biodiversity (Casson et al., 2012; Prowse, 2001b; Thellman et al., 2021; Yang et al., 2020). To understand the impacts of future climate change on river ice development and thus river channel erosion and sediment transport, we must first understand the interplay between river flow velocities and river ice development and decay (Lotsari et al., 2020; Peters et al., 2017; Rouzegar and Clark, 2023).

* Corresponding author.
E-mail address: tuure.e.takala@aalto.fi (T. Takala).

https://doi.org/10.1016/j.jhydrol.2024.132447
Received 28 June 2024; Received in revised form 12 November 2024; Accepted 18 November 2024
Available online 29 November 2024

Understanding the complex process of ice formation requires detailed data about meteorological, hydrological and physiographic properties of the river and its catchment. While the basic initiation of frazil ice development due to supercooling (i.e. water temperature a few one-hundredths of a degree below 0 °C in turbulent flow) is well understood, there are still uncertainties of the impacts of partial ice-cover on flow velocity (McFarlane et al., 2015, 2017). With higher winter temperatures, this cycle of freezing and thawing will happen more often (Andréasson et al., 2004; Lind and Nilsson, 2015), thus this is a particularly important period in the ice cycle to study. Findings from field studies done in full ice-cover conditions during the last decade suggest that ice cover affects the vertical and lateral distribution of flow velocity and in some cases is opposite to the characteristics observed in open-channel conditions (Demers et al., 2011; Lotsari et al., 2017). The roughness of both the river channel and the ice will affect flow velocities. Rough surfaces reduce flow velocities in the immediate vicinity of the rough boundary, while simultaneously increasing the applied shear stress on the rough boundary. This redistribution of flow and shear stress can potentially influence the rates of border-ice growth, both laterally and in terms of thickness, as well as the processes of sediment and ice erosion and deposition (Peters et al. 2018; Clark and Doering, 2009).

However, most of the previous studies on the relationship between hydraulics, supercooling, and frazil ice development during the partial ice cover period have been conducted in flumes (Carstens, 1966; Daly and Crrel, 1984; Clark and Doering, 2009; McFarlane et al., 2015). A better understanding of ice cover formation and decay processes (i.e. periods of partial ice cover) in natural rivers, together with different flow situations, is a key first step in enabling predictions of future climate change impacts on northern rivers and subsequent interactions with sediment transport.

The availability of field data under partial ice-cover conditions are limited due to the temporary nature of border ice growth and the low strength of thin ice, which raises safety concerns for data collection (Nyantekyi-Kwakye et al., 2020). Similarly, there is a scarcity of numerical modeling studies on partial ice cover, primarily due to the lack of sufficient benchmark data for model validation (Rouzegar and Clark, 2023). In order to observe the impact of partial river ice on flow velocities, new methodological development was needed. During the freezing period, the river ice is not thick enough for doing measurements by standing on the (border) ice, and boat-based flow velocity measurements are not possible as it may affect river ice development conditions. One solution is close-range remote sensing, such as image velocimetry methods that enable analysis of surface flow velocity between consecutive video frames (Rohacs et al., 2023). In a study conducted by Michel et al. (1982), the surface water velocity was determined by tracking ice floes from film sequences at the St. Anne River in Quebec. This was one of the first studies using video-based velocity analyses for rivers. The particle image velocimetry method first appeared in the literature in 1984 (Adrian, 1984, 2005). Since then, these methods have developed, and multiple approaches are available that suit different types or quality of video data and research questions. (Large Scale) Particle Image Velocimetry ([LS]PIV) detects particle groups (Yeh et al., 2019), Particle Tracking Velocimetry (PTV) detects individual particles (Eltner et al., 2021), and Space-time Image Velocimetry (STIV) detects changes of pixel values (Zhao et al., 2021), for example, differences in brightness or actual particles moving through the images. STIV has great potential in real-time monitoring of river flow with its high spatial resolution and its ability to provide flow measurements efficiently and simply, reducing the complexity of time-related analyses (Watanabe et al., 2021; Zhao et al., 2021). The method hinges on the analysis of space–time images (STIs), which are generated by stacking sequential image lines or columns extracted over time, usually perpendicular to the flow direction (Fujita et al., 2007). PIV has recently been used in seepage analyses in the case of ice jams (Murray et al., 2022). However, to our knowledge, STIV, or any of the other methods, have not been used to detect changes in river flow velocity along with frazil ice and partial river ice cover formation, or during ice decay, in river systems. However, recent studies from open-channel flow conditions have shown that surface flow velocities, derived from close-range remote video datasets (Eltner et al., 2021), can also be used for discharge calculations with additional reference data, in addition to enhancement of numerical modelling calibration (Wolff et al., 2024).

However, before being able to accurately model freezing and melting periods, we must take the first step to understand the processes based on measured data. Therefore, the main objective of this study is to understand changes in surface flow velocity during freezing causing ice formation and melting periods causing ice break-up of three Nordic rivers. More specifically, we investigate the interplay between surface flow velocity and the initiation and progression of freezing and break-up. The study was conducted in three rivers with reaches having varying characteristics (e.g., slope and depth), representative of boreal and sub-arctic channel types, using video-based surface velocimetry methods (STIV). The temporally dense time series enables the detection of these ice processes and thus allow us to address our study objective. As the three study rivers (Pulmanki River, northern Finland; Koita River, eastern Finland; Sävar River, northern Sweden) are located in regions where a shortened ice-covered period is predicted (AMAP 2011), the results of this study can be used in future research to investigate the effects of climate change on these areas.

2. Study areas

The study includes two rivers in Finland: the Pulmanki River (69.9° N 28.0° E), located in northern Lapland, and the Koita River (62.9° N 31.4° E), situated in eastern Finland in the region of Northern Karelia. The third site is the Sävar River (64.2° N, 20.4° E) in northern Sweden, Västerbotten County. All these areas (Fig. 1) were glaciated under the Fennoscandian ice sheet in the Late Weichselian, and therefore these catchments exhibit geomorphological typical characteristics, including exposed bedrock areas, till, moraine formations, and glaciofluvial deposits and sediment. Data from the Pulmanki and Sävar Rivers were collected in autumn 2021 to spring 2022, and from the Koita River in autumn 2020 to spring 2021.

2.1. Pulmanki River

The upper Pulmanki River, in northern Finland, is situated in the polar region within a subarctic climate characterized by cool and short summers without a distinct dry period (Peel et al., 2007). Peak discharges of up to 70 m^3/s occurs from mid-May to early June due to snowmelt (Kasvi et al., 2015), while summer and autumn discharges average around 4 m^3/s (Kasvi et al., 2012). The river is covered in ice for 7–8 months, from October until late April or May (Lotsari et al., 2019), with an average thickness of 52 cm, which is influenced by the river's flow rate and depth (Kämäri et al., 2017). Ice break-up generally begins with thermal melting, which continues with more mechanical breakup as the ice decays and the river clears (Lotsari et al., 2019). The study area is surrounded by fjelds and the river meanders through a valley filled with glaciofluvial and glaciolacustrine sediments (Hirvas et al., 1988). The vegetation is typical subarctic, consisting of low shrubs and alpine birch. The Pulmanki River has the lowest slope of the three rivers, with a gradient of 0.000122 m/m. Additionally, the river at this site is relatively shallow, as shown in Fig. 3. The maximum water depths recorded were 1.1 m in October 2021 and 2 m in May 2022.

2.2. Koita River

The Koita River, located in eastern Finland, is in the mid-boreal climate zone. Similar to the Pulmanki River, the Koita River experiences increased flow in spring due to snowmelt, but heavy rainfall in summer and autumn can also cause peak flow conditions (Kärkkäinen and Lotsari, 2022). During the open channel period in 2020, the river

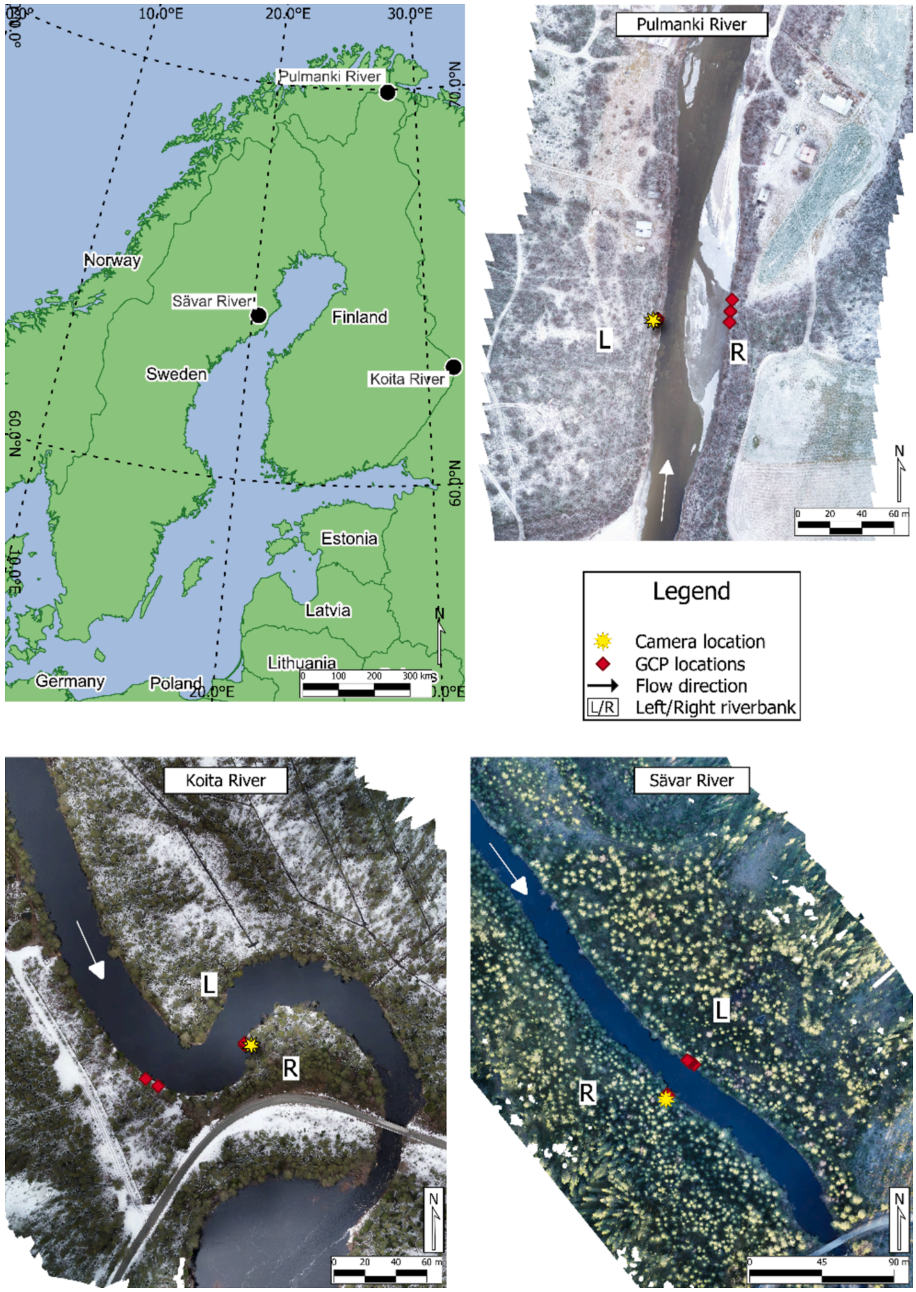

Fig. 1. The study sites and locations of time-lapse trail cameras and the Ground Control Point (GCP) locations for georeferencing the video frames for flow velocity (STIV) analyses. At the Koita River, the GCPs were marked on tree trunks on the far side of the river, but on branches next to the camera.

discharge varied between 7 and 33 m^3/s (Kärkkäinen and Lotsari, 2022). The region has well sorted surficial sediments from a glacial river. Forestry activities, including timber-floating from the 19th century to the 1970s, impacted the catchment, but recent assessments show that it has returned to a natural state (Metsähallitus, 2006). The study site includes a meander bend 170 m upstream of a section of rapids. The river has a low gradient of 0.000615 m/m. The greatest water depth was 3.0 m in the spring of 2021 (Fig. 3).

2.3. Sävar River

The Sävar River, in northern Sweden, is also located in the subarctic climate region. The river has summer low-flow and mid-winter discharges of 5 m^3/s and 3 m^3/s, respectively (Polvi et al., 2020). The highest flow peak, 39 m^3/s, occurred during the spring snowmelt in 2021 (SMHI, 2023). High discharge events occur year-round, first during spring snowmelt and again in late autumn from heavy rainfall. According to Polvi et al. (2020), during mid-winter stable ice cover conditions with an average thickness of 0.56 m, the ice had distinct layers, suggesting multiple freezing events. During ice break-up, higher temperatures and flowing water erode the ice from both the top and bottom. Mechanical break-up further fragments the ice, which, once frozen to the banks, breaks apart and drifts downstream. Similar to the Koita River, there are rapids circa 150 m downstream of the study location. The study area is located in a partially enclosed valley with steep terrace slopes formed by glaciogenic and glacio-fluvial sediments (Polvi et al., 2020). The Sävar River has the highest gradient, with a slope of 0.00135 m/m. Maximum water depth during the observation period was 2.4 m in 2021 autumn, and 1.9 m during June 2022.

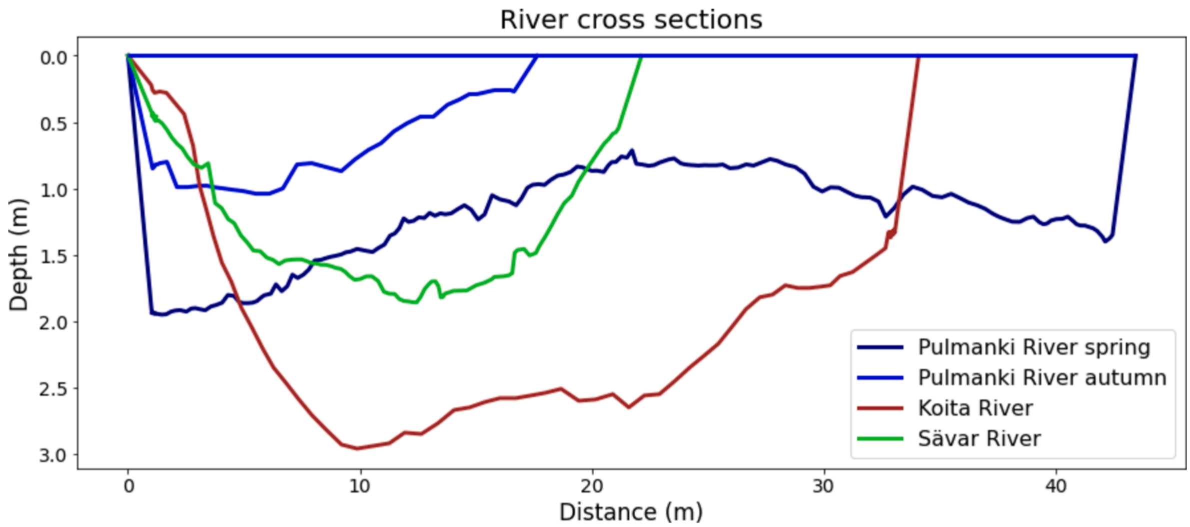

Fig. 2. Cross-sectional profiles of the Pulmanki River (on 16.05.2022, at 39 m^3/s discharge, and on 20.10.2021, at 6 m^3/s discharge), Koita River (on 10.05.2021, at 20 m^3/s discharge) and Sävar River (on 07.06.2022, at 9 m^3/s discharge). The cross-sections of the rivers are from the same spot as where the camera on the river is located (cf. Fig. 1). In the Pulmanki River, ice accumulation along the right bank and a lower water level in autumn prevented a complete echo sounding survey of the entire riverbed.

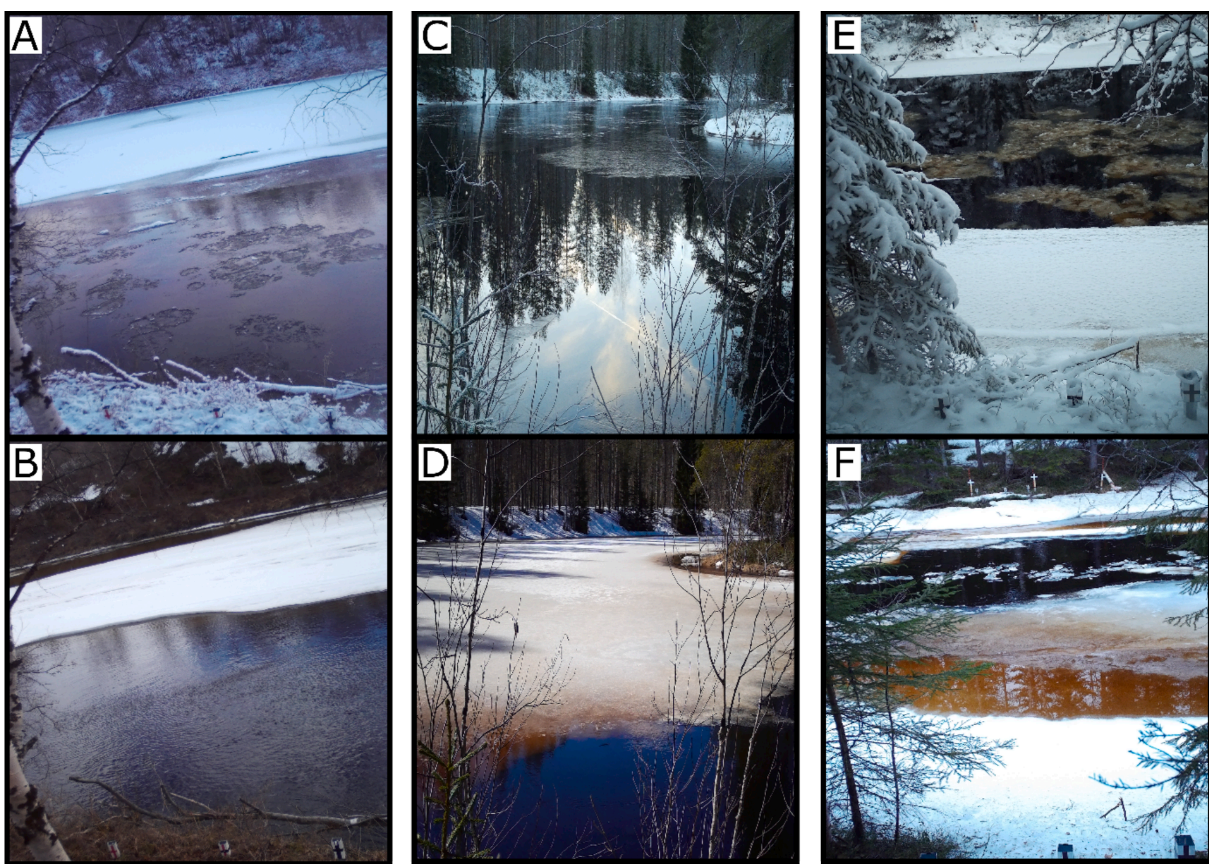

Fig. 3. Pictures from trail cameras, the top row shows a picture during freezing period and the bottom row shows a picture during melting period. Images A and B: Pulmanki River, C and D: Koita River, E and F: Sävar River. Ground control points can be seen in the images as white squares marked with a cross. Pieces of tape can be seen on the branches of the bush along the Koita River, which were also used as ground control points.

3. Materials and methods

3.1. Field measurements

This study was based on measurements from the Koita River in 2020–2021 and the Pulmanki and Sävar Rivers in 2021–2022. Water levels were measured from the cross-section locations (Fig. 1: camera locations) using RTK-GNSS at distances ranging from 50 to 500 m upstream and downstream of the study site to accurately calculate the water surface slope (m/m) (see Appendix A for RTK-GPS measurement accuracies). In the Sävar River, data from a submerged water pressure sensor (Solinst Levelogger), combined with with a Solinst Barologger sensor of air pressure, was used to calculate water depth throughout the study period. RTK-GNSS water level measurements from the autumn and spring allowed us to convert the depth data into water level data for the freezing and melting periods. At the Sävar River site, water temperature was measured using HOBO Onset sensors, while air temperature was measured using the Solinst Barologger and a trail camera. At the Pulmanki River site, both HOBO Onset sensors and a trail camera were used for air temperature, and a Solinst levelogger was used for water temperature. At the Koita River, air temperature was only recorded by a trail camera.

Flow velocity measurements were conducted at the study sites to provide reference data for the remote sensing video data, which are later used for surface velocity calculations (see below). In the Pulmanki River, measurements coincided with the video data collection dates (20.10.2021 and 16.5.2022). For the Sävar River, flow velocity was measured one and a half day before the camera installation (9.11.2021) and again in spring 2022 on the same day as the video data (6.7.2022). At the Koita River, measurements were taken one month before the camera installation in autumn 2020. At the Pulmanki and Koita Rivers, 3D flow measurements were performed with an Acoustic Doppler Current Profiler (ADCP, Sontek M9). Whereas at the Sävar River, an electromagnetic velocimeter (Valeport Model801), which is capable of 1D flow measurements, was used in the autumn 2021 freezing period and an ADCP was used in the spring 2022 melting period. From the ADCP data, the velocity value of the cell closest to the surface was used for the analyses. These cells were ~16 cm below the surface. In the Sävar River (fall 2021), flow velocities were measured with an electromagnetic velocimeter at 2 m intervals across the transect, approximately 5 cm from the surface.

3.2. Time-lapse camera installation

video data were collected using time-lapse trail cameras at each study site (Fig. 3). Battery-powered Burrel Edge HD cameras were mounted on large trees to minimize wind movement and capture a cross-sectional view of the river channel, ensuring visibility of both banks for reference measurements. The cameras recorded 10-second video clips every two hours at a resolution of 1920x1080 pixels and 30 frames per second. Ground Control Points (GCPs) were placed on both sides of the channel as reference points in the cameraman's field of view. Where possible, GCPs were placed on the ground close to the riverbanks; however on the Koita River, GCPs were attached to nearby trees and branches. The GCPs were measured with a Trimble R12i RTK-GNSS (Real-Time Kinematic Global Navigation Satellite System) and are used to correct any camera frame movement (see Appendix A for GCP measurement accuracies).

3.3. Open source data

Reference air temperature data were obtained from nearby national weather stations, and historical averages (Pulmanki 1984–2021, Koita 2000–2020, Sävar 1989–2021) were calculated for comparison with measured temperatures during the study period (See Section 3.1). Finnish data were obtained from the Finnish Meteorological Institute (FMI), with the closest station to the Pulmanki River located in Nuorgam, Utsjoki, about 18 km from the study site. The closest weather station to the Koita River site was Mekrijärvi, Ilomantsi, 28 km away, while air temperature data for the Swedish site was obtained from a Swedish Meteorological and Hydrological Institute's (SMHI) station 29 km away.

Discharge data for the entire measurement period of the Sävar River was obtained from an SMHI hydrological station located approximately 9 km upstream of the Sävar River study area (Swedish Meteorological and Hydrological Institute, 2023). At this station, a sensor continuously monitors water level, and these data were used to calculate discharge through a stage-discharge curve. To ensure accuracy, periodic reference measurements are conducted to recalibrate the curve (Swedish Meteorological and Hydrological Institute, 2024). Note that flow velocity measurements for sävarå and other sites, were based on own measurement, not from national sensor networks.

3.4. Velocity and ice cover analyses from video data

The cameras recorded videos from the rivers every two hours. Some footage was discarded due to environmental disturbances, including lack of daylight in late autumn and early spring, fog, heavy snow, rain and strong winds that obscured the view. After filtering out unusable footage, the remaining videos were extracted as frames for analysis of surface flow velocity and ice cover.

Surface flow velocity analyses were performed using Hydro-STIV software (Hydro-STIV v.1.2.2, Hydro Technology Institute co.), which uses Space-Time Image Velocimetry (STIV) for velocity estimation, a method derived from Large-Scale Particle Image Velocimetry (LSPIV) developed by Fujita in 2007 (Fujita et al., 2007). The videos were georeferenced using known GCPs and the software performed orthorectification and calibration, providing error values (see Appendix B for error values) related to GCP accuracy, camera lens distortion, image quality, lighting, and human error. The method relies on analyzing space–time images (STIs), created by stacking sequential image lines or columns, usually perpendicular to the flow (Fujita et al., 2007), which captures temporal and spatial flow variations. Velocity is estimated by examining changes in pixel brightness from moving objects, such as leaves or ice. Advanced filtering and deep learning algorithms enhance the accuracy and robustness of these measurements, particularly in challenging conditions. A study by Watanabe et al. (2021) showed that deep learning can increase the efficiency and performance of STIV by continuously improving with more data, while also saving time through automation, especially in large-scale analyses. The software allows users to create search lines composed of points where analysis is performed on their videos. Along the Sävar River (width: ~21 m) and the Koita River (width: ~34 m), search lines were placed in the STIV software at 40 cm intervals, while the wider cross section of the Pulmanki River (width: ~42 m) required search lines at 50 cm intervals.

In STIV, flow velocity v is calculated using the gradient φ of the stripe pattern in the space–time image, representing water surface movements (Fig. 4). Pixel changes in the video capture these dynamics, and Eq. (1) uses a proportional coefficient k to convert pixel measurements to real-world scale.

$$v = ktan\phi \tag{1}$$

To achieve automatic detection of STI pattern gradients, a Convolutional Neural Network (CNN) was used to accurately approximate the nonlinear function $f(I)$, which calculates the gradient ϕ of the stripe pattern [2] based on the STI information $I \in \mathbb{R}^{Ch\times H\times W}$. In this context, Ch represents the number of channels in the STI, which is 3 for an RGB image. H denotes the height of the STI, indicating the number of image frames that compose the STI. Lastly, W signifies the width of the STI, representing the number of pixels in the search line.

$$\phi = f(I) \tag{2}$$

A CNN was employed to approximate the pattern gradient's classification probability distribution p when the image intensity value information I is given as shown in Eq. (3), and then the estimated gradient ϕ is $\widehat{\phi} \in \{\phi_1, \phi_2, \cdots, \phi_N\}$ which gives the maximum probability.

$$\phi = argmax_{\hat{\phi}} p(\widehat{\phi}|I) \tag{3}$$

The use of the CNN method enables the estimation of gradient values and the production of estimated probability distributions for each class. Additionally, the software evaluates the confidence intervals of the

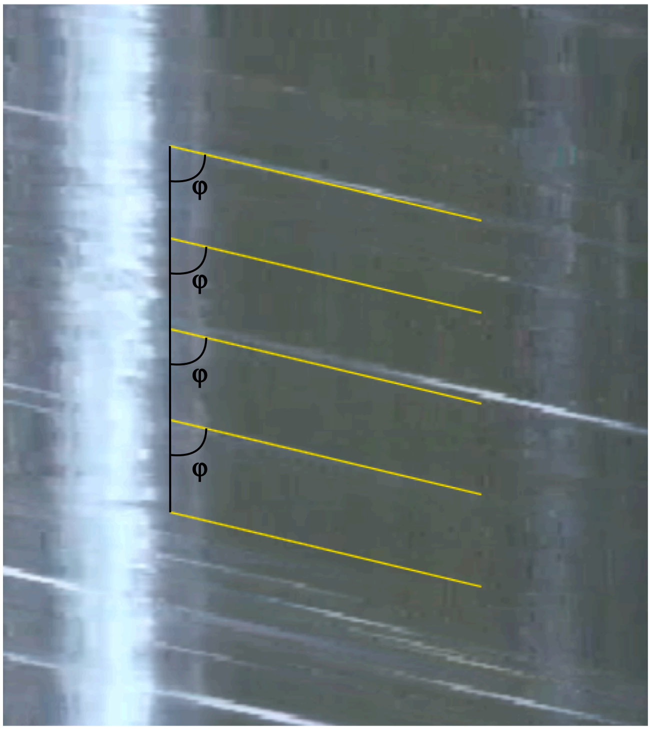

Fig. 4. Stripe pattern seen on space–time image. The white lines in the image represent objects moving on the river's surface, which appear as lines in the space–time image. Wind-induced waves can complicate the analysis if there are no distinctive features on the water surface, creating curved lines.

gradient values, taking into account the uncertainties associated with the probability distributions. The Hydro-STIV software is based on the approach described by Watanabe et al. (2021) but has been further developed. The current version includes a CNN trained on 40,000 STIs to improve resolution and performance, which we used for our analyses (Hydro Technology Institute co., 2022)

Analyzed surface velocities were compared with field measured values to validate the results. STIV-derived velocities were compared with ADCP measurements from all three rivers. Reference measurements were compared with image-based velocity analysis using the Mean Absolute Percentage Error (MAPE) for cross sections, where lower MAPE values indicate better accuracy. At the Pulmanki River, the MAPE was 17.81% in the autumn 2021 and 5.58% in the spring. At the Sävar River study site in autumn 2021, sparser velocimeter reference points and a 1.5-day gap between measurements and video analysis led to a high MAPE value of 47.05%; in the spring of 2022 the MAPE for the whole cross section was 8.54%. At the Koita River study site, a significant time lag between measurements and video analysis prevented a reliable comparison of STIV and ADCP velocities. However, the spring measurements at the other two sites were consistent, confirming the effectiveness of the method and that the Koita River data can be also used. Autumn discrepancies were due to technical problems, different equipment, natural flow variations and environmental factors such as the movement of frazil ice under the ADCP sensor.

The same search lines, as used for the surface flow velocity calculations, were used for the ice cover detection. Ice cover, i.e. the percentage of ice cover over the channel width, was examined visually at the points located on the search line. At each time point from the beginning of each video (i.e. the image of the first frame) the amount of ice cover across the channel was calculated as a percentage of the total channel width.

3.5. Statistical analysis of parameters during freezing and melting periods

To understand the potential interlinked impacts of multiple parameters during freezing and melting periods, the Sävar River was chosen for detailed statistical analysis, because this site had the most comprehensive dataset due to the presence of several sensors in the area throughout the measurement period. Surface flow velocities, air and stream temperature, discharge, water level, and ice extent were examined using correlation analyses and multiple linear regression analysis separately during autumn and spring to determine potential associations with changes that occur during the freezing and melting periods. Spearman's rank correlation was first used to explore relationships between variables, followed by a multiple linear regression models to explain variability in ice extent, with only surface velocity and air temperature as independent variables due to collinearity with other parameters.

4. Results

4.1. Ice-cover development and related velocities in autumn periods

4.1.1. River ice development in the three study sites during autumn

Freezing of the Pulmanki River began on the night of 18th–19th October 2021, with air temperatures near −3 °C, resulting in a 30% increase in ice coverage overnight, influenced by the river's low water level and nearly stagnant conditions on the right side of the river (Fig. 5A). The initial rapid freezing spanned the first two nights, after which the process predominantly occurred during colder nights, with less than a 7 percentage point increase nightly, and minimal freezing during daylight. Frazil ice first appeared during this initial freezing phase. A significant temperature drop to −15 °C on the night following 19th October accelerated frazil ice formation, which was clearly visible by 20th October. After a brief warming on 21st October, temperatures plummeted again on 23rd October to −13 °C, with abundant frazil ice, continuing until the river channel was approximately 85% frozen by 28th October and finally fully frozen in 10 days.

At the Koita River, ice rafts and frazil ice formation began as air temperatures dropped <0 °C on the nights of 21st and 22nd November 2020. A temperature drop to below −5 °C on the night before 26th November led to frazil ice. Ice rafts persisted until 3rd December, with new appearances on 4th and 5th December despite stable temperatures. A sharp decrease in temperature to <−12 °C on the night of 7th–8th December initiated substantial freezing, resulting in a thin ice layer covering 43% of the channel by the morning of 8th December, which expanded to full coverage by the next morning as temperatures remained low.

Freezing on the Sävar River commenced on 14th November 2021 but was interrupted by melting during a warmer period two days later. Freezing resumed on 19th November, with the river approximately 15% frozen by the night of 21st–22nd November. However, over the next two days, ice coverage decreased to about 6% before the freezing rate increased. From 24th November onwards, daily freezing rates varied between 2% and 11% coverage, primarily occurring during nighttime. Water rose to the ice's shoreward edge on several days during the freezing process (Fig. 5C shows a spike starting from 26th November). The entire river cross-section was completely frozen by 6th December, culminating in an 18-day ice formation. Frazil ice was prominent from 26th November to 2nd December, with air temperatures on 26th November dropping and reaching −21 °C the following night, leading to the largest observation of frazil ice on 27th November. Thereafter, only very thin ice rafts were noted until the river was fully frozen.

As a result, all rivers experienced rapid freezing as air temperatures allowed. This progression was steady at the Pulmanki and Sävar Rivers, although the Sävar River experienced minor ice development fluctuations during its freeze-up period. The Koita River, in contrast, froze exceptionally quickly within two days, a stark difference from the 10 and 18 days observed in the other two rivers. Notably, frazil ice and ice rafts were a common occurrence in all three rivers. At the Koita River, the frazil ice was notably smaller and less frequent than on the other

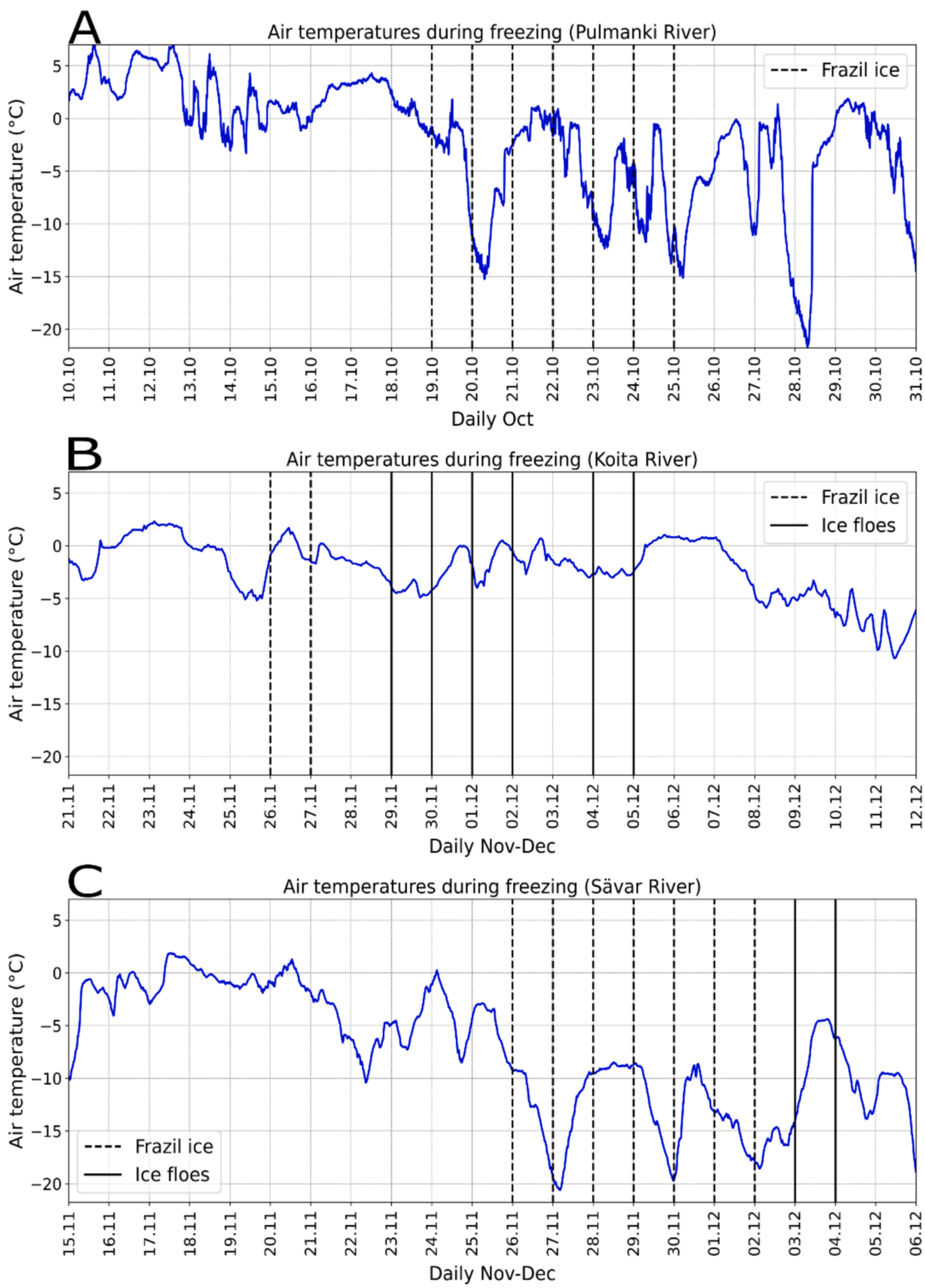

Fig. 5. Air temperatures during freezing in three studied rivers: A Pulmanki River, B Koita River and C Sävar river. Vertical dotted line show when frazil ice and vertical blue lines show when ice floes were observed during freeze-up.

rivers. At the Sävar River, abundant frazil ice appeared after one particularly cold night with air temperatures reaching as low as −21 °C, after which such low temperatures persisted for 7 days together with frazil ice. At the Pulmanki River, there were greater temperature fluctuations, which resulted in the occurrence of frazil ice and ice rafts; during the first freeze some frazil ice was observed but after the night-time temperature dropped to −15 °C, more and larger frazil ice was seen for seven consecutive days.

4.1.2. *Velocities during the autumn ice-cover development period*

At the Pulmanki River, maximum surface velocities prior to freezing on 18th November fluctuated between 0.95 m/s and 1.3 m/s, averaging at 1.18 m/s (Fig. 6A). Trail camera footage taken on 17th October showed the water rising and submerging a central sandbar. By 19th October, the water receded, exposing the sandbar, with subsequent images indicating a stable water level. The onset of rapid freezing initially had minimal impact on flow velocities due to the quick freeze-up of the shallower bank, which did not affect the deeper bank side.

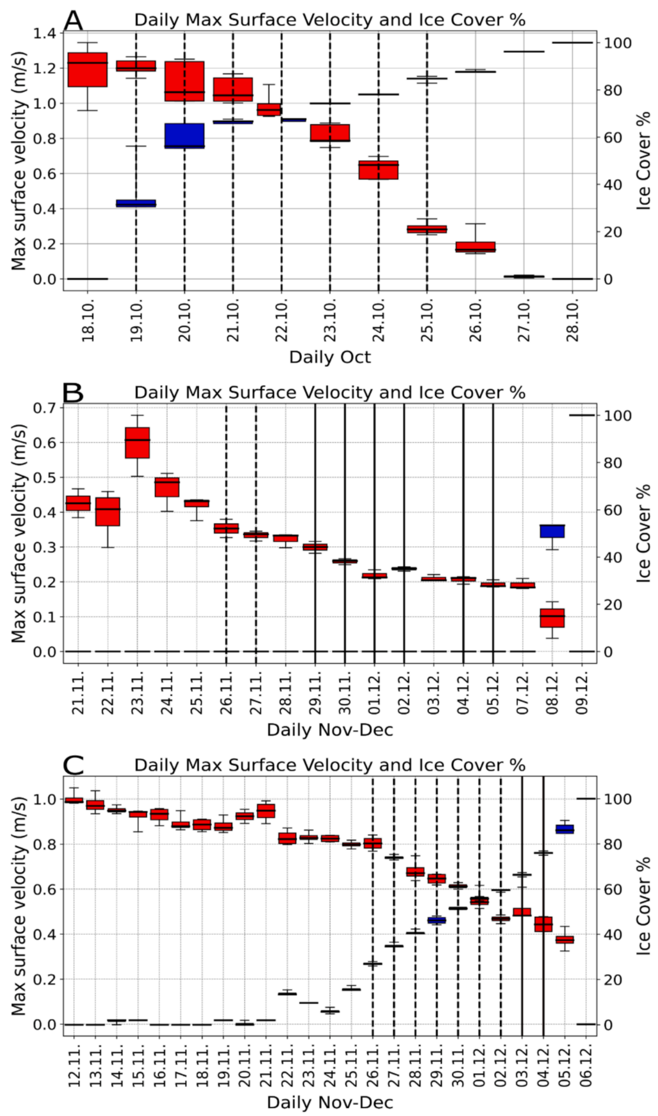

Fig. 6. The maximum surface flow velocity (red) and ice cover % (blue) of the cross-section from A) Pulmanki River 18.10.2021–28.10.2021, B) Koita River 21.11.2020–09.12.2020, and C) Sävar River 12.11.2021–06.12.2021. Ice cover was observed from time-lapse pictures every two hours (during the periods when there was sufficient daylight). Vertical lines indicate when frazil ice was observed in the river. Ice developed rapidly during the first three days, after which the freezing slowed down and stabilized. In the Pulmanki river, as the ice cover exceeds 60%, a rapid decline in flow velocity is observed. In the Koita River, flow velocity was in a steady decline before the freezing. The ice cover developed within two days. In the Sävar river, a steady decrease in velocity is observed as the ice coverage increases.

However, as freezing progressed to the deeper side of the channel (Fig. 2, Pulmanki River autumn cross-section) around 22nd October, flow velocities began to decline from an average of 0.98 m/s to 0.82 m/s by 23rd October. This decrease continued, with velocities dropping significantly to 0.63 m/s by 24th October and reaching as low as 0.013 m/s just before the river was fully frozen on 28th November. This progression illustrates a marked reduction in flow velocities as the freezing in the channel increased, with the most notable decreases observed once the deeper portions of the channel cross-section began to freeze.

At the Koita River, prior to the initial frazil ice formation on 26th of November, flow velocities ranged from 0.38 m/s to 0.44 m/s, with an average of 0.42 m/s (Fig. 6B). During the formation of the first ice rafts, the average daily maximum surface velocities decreased from 0.35 m/s on 26th of November to 0.22 m/s by 1st of December. From 2nd to 7th December, the mean velocity stabilized between 0.23 m/s and 0.19 m/s, before a significant decrease on 8th December to a mean daily velocity of 0.094 m/s. By 9th December, the river was entirely frozen, marking the end of observable velocities. This pattern underscores a steady decrease in flow velocities leading up to the complete freezing of the river. By examining trail camera images, we observed that the water level steadily decreased slightly (a minor decline can be distinguished in the images). However, estimating the magnitude of this decrease solely from these images is not possible.

At the Sävar River, prior to freezing, the daily maximum surface flow velocities fluctuated between 1.04 m/s and 0.94 m/s, averaging 0.98 m/s (Figs. 6C and 7A). The initial minor freezing events on 14th and 15th of November did not significantly affect the flow velocities, which

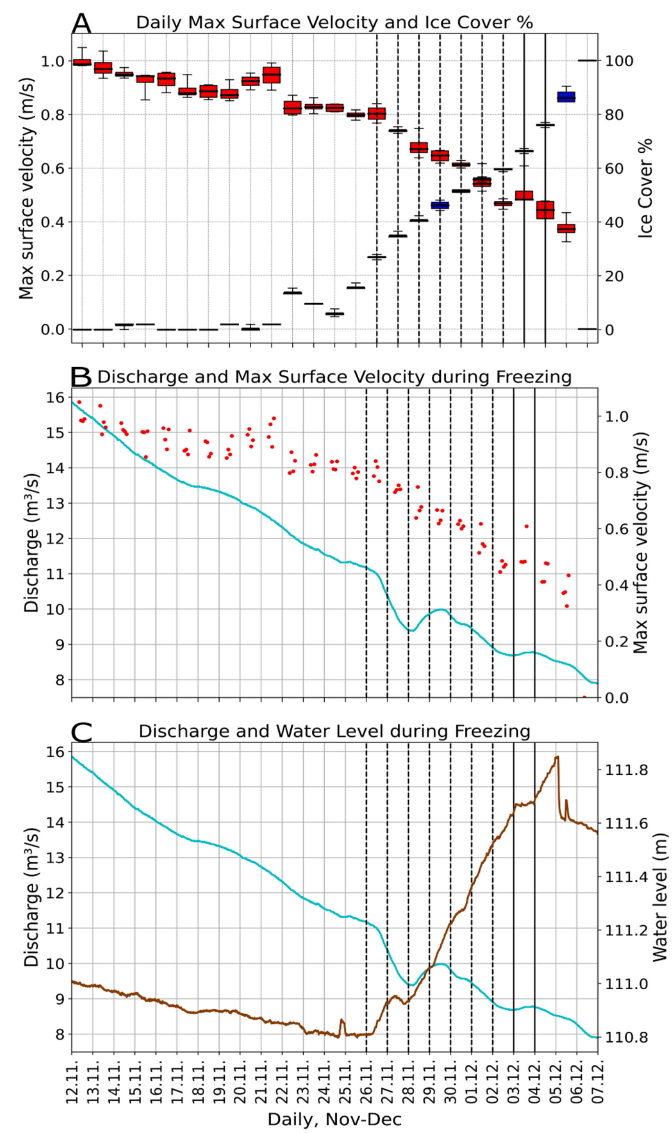

Fig. 7. A) The maximum surface flow velocity (red) and ice cover % (blue) of the cross-section, and B) discharge (turquoise) and max surface velocities (red), and C) discharge (turquoise) and water level (brown) from the Sävar River 12.11.2021–6.12.2021. Vertical dashed lines represent the days when frazil ice was observed. Blue vertical line represents the days that ice floes were observed. In Figure A, a steady decline in flow velocity is observed while the ice cover expands consistently. In Figure B, discharge decreases simultaneously with flow velocity. However, small changes in discharge do not appear to affect the flow velocity (e.g., the change in discharge on 28.11.21); e.g. in (C) the water level rises despite the decrease in discharge starting from 26.11.21.

remained between 0.95 m/s and 0.88 m/s. A notable reduction in flow velocities occurred on 22nd November, with the average dropping to 0.83 m/s. Subsequently, the mean velocities stabilized between 0.83 m/s and 0.82 m/s, even as the ice briefly melted and began to refreeze on 25th November. From that point, as the ice cover on the river expanded, the flow velocities consistently decreased. By 5th December, the day before the river was fully covered in ice, the average daily velocity was recorded at 0.37 m/s, demonstrating a gradual decrease in flow velocity as the freezing progressed. According to the pressure sensor, the water level was nearly 20 cm lower than the autumn peak flow between 13th and 24th November. The gauge located upstream also indicated a decreasing flow discharge. Data from the pressure sensor showed a spike starting on 26th November.

For showing how the surface velocities varied along with ice development at each time step within the cross-section, surface velocities derived from STIV were converted into plots from each time step and then compiled into videos (GIFs), found in the research data (doi.org/10.5281/zenodo.14102870). Due to the large volume of analysis, in addition to including all velocity plots and videos in the research data; figures of flow velocities from around mid-day of each measurement day were used, as that time always had the best lightning conditions. The resulting videos effectively illustrate how velocities changed and how the flow field narrowed as freezing progressed. This visualization enhances the resolution of how velocities change across the cross-section during freezing.

4.2. The ice-cover break-up and related velocities in spring periods

4.2.1. River ice melting at the three study sites during spring

Water was first observed on the ice cover at the Pulmanki River on 24th April. Despite a brief air temperature drop below −8 °C on 26th April, melting resumed with temperatures staying above 0 °C from 1st May onwards, leading to a gradual edge melt and the appearance of cracks. The first significant ice break occurred on 5th May, marking the onset of rapid ice breakup. Over the next 6 days, melting rates varied, with the ice breakup accelerating and the last stable ice disappearing by 11th May, culminating in an 11-day period from the onset of flowing water to complete ice clearance.

The initial melting on the Koita River was noted on 10th April, with water rising onto the ice at the left bank, making the ice edge on the right bank barely visible. Melting accelerated dramatically by 13th April, with water flowing at the right bank's edge. On 14th of April, approximately 17% of the ice broke off, followed by a 26% reduction overnight. By the evening of 15th of April, the cross-section was entirely ice-free, although some ice remained at the downstream end of the meander bend upstream of the cross-section. The entire process from the first signs of melting to complete ice clearance from the cross-section took 6 days.

The initial ice movement at the Sävar River was observed on 19th of April, with a crack appearing that widened, and flowing water was visible by 20th of April. Ice melting was initially slow, with only a 4% reduction by 21st of April, but a significant air temperature increase to 12 °C on that day marked the beginning of rapid melting. On 22nd of April, 18% of the ice cover melted away, and by 23rd of April, the most substantial melting occurred, clearing 48% of the cross-section. Large ice floes began moving downstream, significantly opening up the channel. By 29th of April, all ice had melted from the Sävar River, completing the melting process within 11 days.

The ice melting processes at the Pulmanki, Koita, and Sävar Rivers showcase both similarities and differences in their responses to spring thaw conditions. All three rivers experienced a period of rapid melting and ice break-up after initial signs of thaw, indicating a common influence of rising air temperatures on accelerating ice breakup. However, the duration from the onset of melting to complete clearance varied, with the Koita River melting most rapidly within 6 days compared with 11 days at the other sites, highlighting a notable difference in the impact of local environmental and climatic conditions. Furthermore, while the Pulmanki and Sävar Rivers took a similar amount of time to clear completely, the pattern and speed of ice melt diverged, emphasizing the unique interplay between temperature increases and the physical characteristics of each river. These variations underscore the complexity of river ice dynamics and the critical role of specific geographical and meteorological factors in shaping the spring ice melt cycle.

4.2.2. Velocities during the spring ice-cover thawing period

At the Pulmanki River, the first observed flowing water was seen on the evening 1st of May, with a calculated (with STIV) velocity of 0.38 m/s (Fig. 8A). By 3rd of May, the flow velocity steadily increased, with velocities averaging 0.56 m/s. A marked rise occurred by 6th of May, with the flow peaking at 1.26 m/s. The trend of increasing velocities

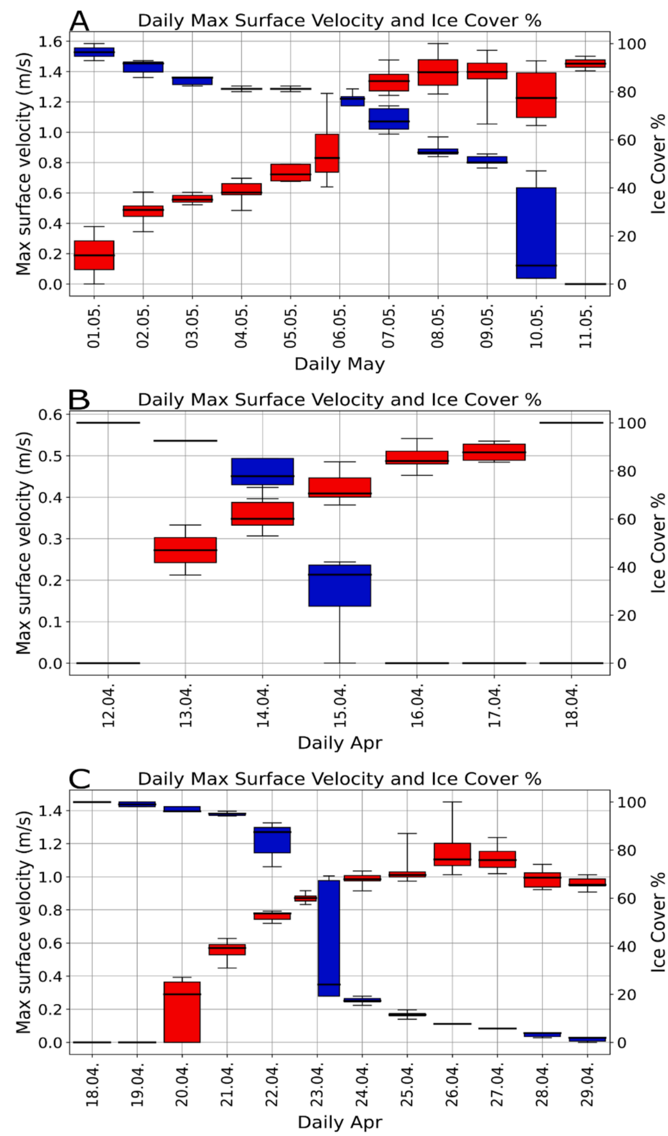

Fig. 8. The maximum surface flow velocity (red) and ice cover % (blue) of the cross-section from A) Pulmanki River 1.5.2022–11.5.2022, B) Koita River 12.04.2021–18.04.2021, and C) Sävar river 18.04.2022–29.04.2022. In the Pulmanki River, the ice melted steadily at first, but on 10.5.22, a large portion of the ice broke off and opened the channel. The flow velocity initially increased gradually, but on 6.5.22, it experienced a surge. In the Koita River, the ice started melting on 13.04.21, and on 15.5.21, the largest ice pieces broke off and were carried away by the current. The flow velocity development remained steady from that point onward, once flowing water was observed. In the Sävar River, the velocities increased consistently as the ice began to melt in the river.

culminated on 8th of May, with the highest recorded average of 1.39 m/s for the period. Following this peak, a gradual decline commenced, and by 10th of May, the average velocity had reduced to 1.25 m/s, coinciding with the complete melting of river ice. Despite limited measurements on 11th of May due to poor weather, the remaining high velocities suggested a stabilization after thawing.

At the Koita River, initial flow velocities were measured from an opening on the channel's right bank on 13th of April, with initial velocities of 0.21 and 0.33 m/s (Fig. 8B). The following day, velocities increased, averaging 0.36 m/s. A further rise was observed on 15th of April, with velocities averaging 0.42 m/s, which also marked the complete melting of the observed cross-section. The thawing continued to influence the flow, leading to higher velocities up to 0.54 m/s by 16th of April and maintaining an average of 0.51 m/s by 17th of April, when the entire meander bend had melted.

Flow velocity measurements on the Sävar River began on 20th of April amidst the widening of a central crack, starting with velocities ranging from 0.2 to 0.39 m/s (Fig. 9A). From 21st of April to 26th of April, as the ice continued to melt, there was a noticeable increase in flow velocities, with a significant rise to an average of 0.76 m/s by 22nd of April. The trend of increasing velocities peaked on 26th of April with a daily average of 1.17 m/s, coinciding with the river being nearly ice-free. Following this peak, the velocities began to decline, stabilizing around 1.02 to 1.234 m/s by 27th of April, and further decreasing by the end of the observation period on 29th of April, as the river became completely ice-free, with velocities ranging from 0.91 to 1.01 m/s.

The spring thaws of the Pulmanki, Koita, and Sävar Rivers revealed a consistent increase in flow velocities, with each river reaching its peak as the ice melt progressed. The Pulmanki River showed the highest velocity peak, while the Koita River had a more gradual increase, peaking at a lower velocity. In contrast, the Sävar River displayed a rapid rise to its peak velocity. All rivers experienced a stabilization and subsequent decrease in velocities as the thaw completed, indicating a shared response to environmental conditions following the peak. The differences in peak flow velocities and the timing of these peaks suggest varying local geographical or meteorological influences on each river's thawing dynamics.

Similarly as for autumn, videos of springtime velocity changes for each time step are found in the research data (doi.org/10.5281/zenodo.14102870) including figures from images during mid-day of each analyzed day. The videos show how surface velocities increase, and as the ice melts, the flow field expands. These videos also show how flow velocities vary with the distance from the channel bank and the ice edge. This enhances the resolution of how velocities change across the cross-section during melting.

4.3. Statistical analysis between temperatures, river flow, water stage and ice characteristics at the Sävar river

4.3.1. Correlation results and multiple linear regression models from the Sävar River

Based on the Spearman's rank correlation coefficients between the six measured variables (ice cover, air temperature, max surface velocity, water level, discharge, and water temperature) during the freezing

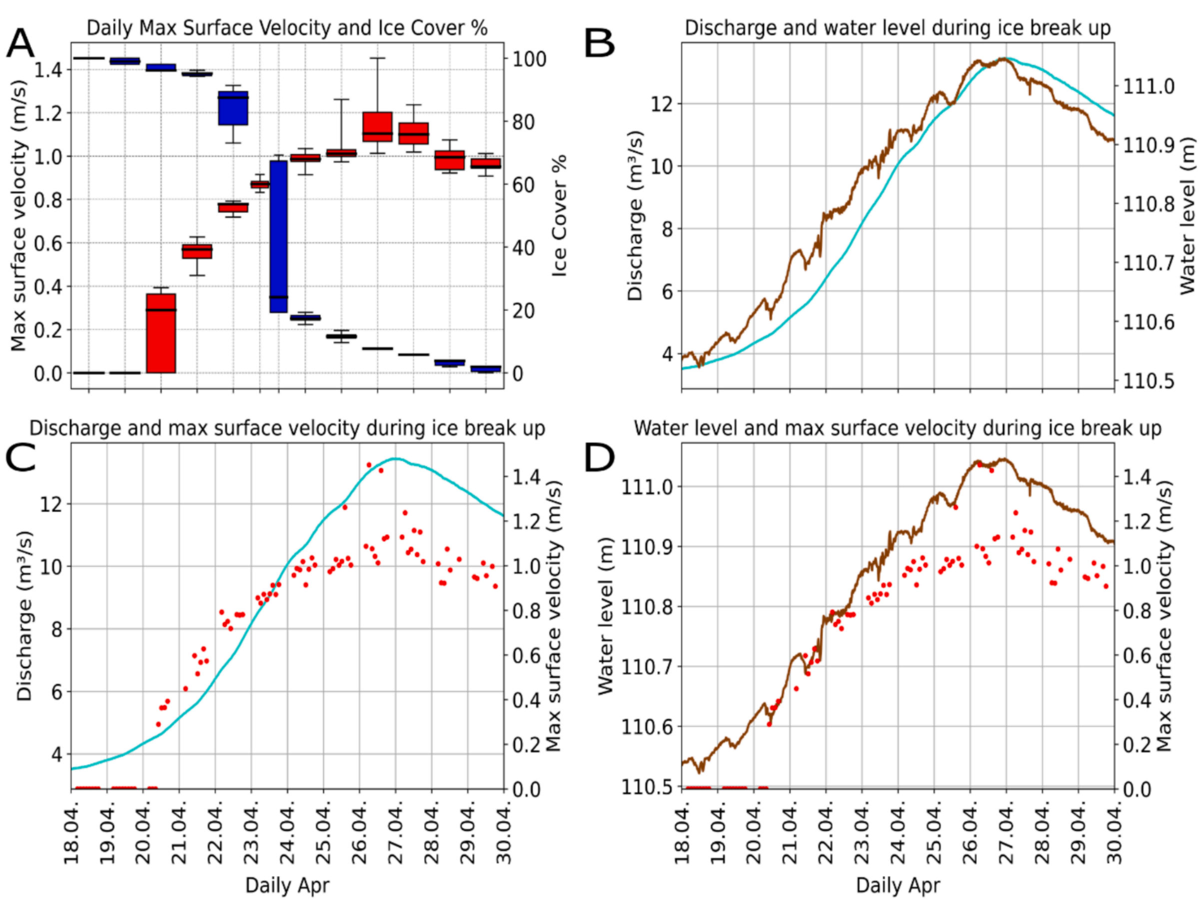

Fig. 9. A) The maximum surface flow velocity (red) and ice cover % (blue) of the cross-section, and B) discharge (turquoise) and water level (brown), C) discharge (turquoise) and max surface velocity (red), and D) water level (brown) and max surface velocity (red) from the Sävar River during ice break up, 18.4.2022–30.4.2022. In Figure A, the flow velocity increases steadily, reaching maximum speeds when only about 10 percent of the ice remains (26.4.22), followed by a slight decrease in velocity. In Figure B, it is observed that the water level and discharge closely follow each other. In Figures C and D, it is observed that the maximum velocity also closely follows discharge and water level.

periods, significant correlations were found among various environmental factors affecting river dynamics at the Sävar River (Fig. 10A). Notably, ice coverage demonstrated an inverse relationship with maximum surface velocity, discharge, air temperature, and water temperature, while being positively associated with water level. Air temperature was positively correlated with maximum velocity, discharge, and strongly with water temperature. Discharge showed a positive correlation with maximum velocity, air temperature, and water temperature, and an inverse relationship with ice coverage and water level. Additionally, maximum velocity and water level exhibited a moderate negative correlation. Water temperature exhibited strong positive correlations with air temperature and discharge, and a notable positive correlation with maximum velocity.

During the melting period (Fig. 10B), ice coverage was negatively correlated with maximum velocity, water level, and discharge. This suggests that periods of lower ice coverage are associated with higher

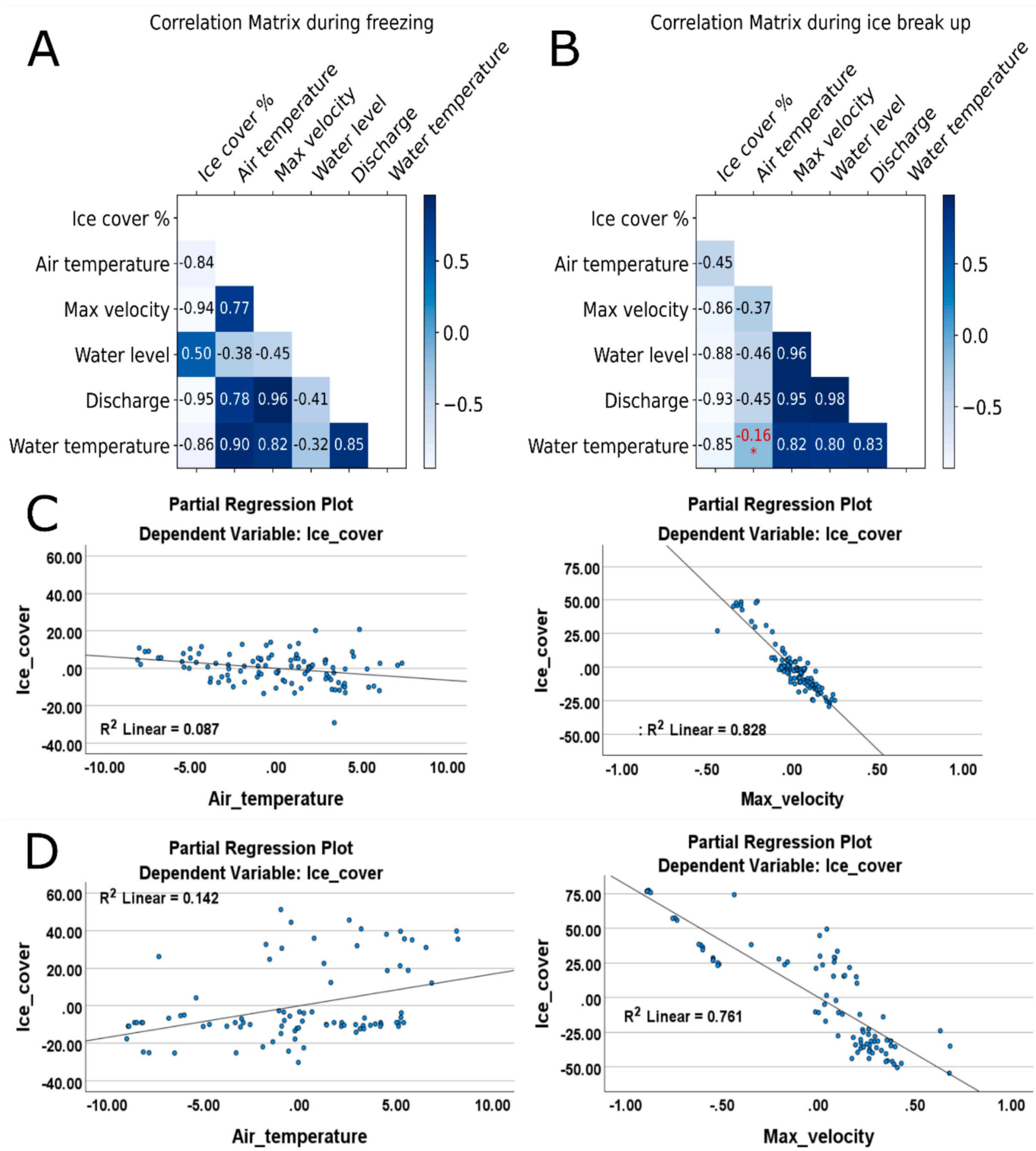

Fig. 10. A) Correlation matrix during freezing, all correlations were significant (p < 0.001), B) Correlation matrix during ice break up, all correlations were significant (p < 0.001) except for one, which is shown in the graph in red with an asterisk (p > 0,1), C) Partial regression plots from the multiple linear regression during the freezing period, and D) partial regression plots from the multiple linear regression during the melting period. From Figure A, it can be observed that during both autumn and spring, the freezing and thawing periods, ice cover has strong negative correlations with air temperature, maximum surface velocity, and discharge. In Figure B, the partial regression plots show that during the freezing period, ice cover has a weak positive relationship with air temperature and a strong negative relationship with maximum surface velocity. Figure C shows that during the melting period, ice cover has a moderate positive relationship with air temperature and a strong negative relationship with maximum surface velocity. From Figure A, it can be observed that during both autumn and spring, the freezing and thawing periods, ice cover has strong negative correlations with air temperature, maximum surface velocity, and discharge.

flow velocities, elevated water levels, and increased discharge. Air temperature was negatively linked with maximum velocity, discharge and water level, implying that temperature variations influence river dynamics. Furthermore, maximum velocity and water level both showed a strong positive relationship with discharge, emphasizing their roles in determining river flow rate, with water level being a particularly significant factor in the river's discharge capacity.

The linear regression model during freezing (Fig. 10C) explained 92.9% of the variance in ice cover ($R^2 = 0.929$, Adjusted $R^2 = 0.928$; standard error: 7.670F(2, 99) = 651.774, $p < 0.001$). Air temperature had a negative impact on ice cover (B = −0.634, Beta = −0.122, p = 0.003), while max surface velocity had a strong negative impact (B = −122.841, Beta = −0.870, $p < 0.001$). Multicollinearity was not a concern, as indicated by acceptable tolerance (0.450) and VIF values (2.222) for both predictors.

The linear regression model from spring during thawing (Fig. 10D) accounted for 80.4% of the variance in ice cover ($R^2 = 0.804$, Adjusted $R^2 = 0.800$SEE = 19.031,F(2, 85) = 174.571, $p < 0.001$). Maximum surface velocity had a strong negative effect on ice cover (B = −81.430, Beta = −0.824, $p < 0.001$), while air temperature had a positive effect (B = 1.687, Beta = 0.188, $p < 0.001$) (Fig. 10C). Multicollinearity was not an issue, as indicated by high tolerance (0.916) and low VIF values (1.091) for both predictors.

5. Discussion

The main objective of this study was to analyze the changes in surface flow velocity during freezing periods with river ice formation and melting periods with ice break-up in three northern rivers. The aim was to detect the interplay between surface flow velocity and the initiation and progress of freezing and break-up, considering varying river characteristics. Using video-based surface velocimetry methods (STIV) and a temporally dense time series, we observed variations in the interaction between ice cover and flow velocities among these rivers.

We found that the most rapid interactions between ice and flow velocities during the autumn freezing period were observed at the Pulmanki River, where velocities declined quickly when ice covered around 70% of the channel. In contrast, the reduction in flow velocity was more gradual in the Sävar and Koita Rivers, which are almost at the same latitude. However, the Koita River is slightly further south and experiences more continental climate conditions than the Sävar River. The rapid decline in flow velocity at the Pulmanki River can be attributed to the closing of the channel and the increase of the wetted perimeter, leading to increased friction due to the rough ice edge. As the ice advances, its impact on the distribution of surface flow velocities becomes clearly visible (doi.org/10.5281/zenodo.14102870). Peters et al. (2018) suggested that the redistribution of flow and shear stress could potentially influence the rates of border-ice growth (both laterally and in terms of thickness); however, we did not observe this phenomenon. Instead, we found that ice development could have influenced the surface flow velocities. As shown in 7B, a decrease in discharge leads to a reduction in surface flow velocity; therefore, the decrease in discharge and the friction caused by ice can together influence flow velocity, which in turn facilitates freezing. The friction caused by the ice was observed in the reduced flow velocities near the ice edge. According to Lotsari et al. (2017), Polvi et al. (2020), and Demers et al. (2011, 2012), the high-velocity core moves towards the riverbed when the river is fully ice-covered, leading to lower flow velocities at the surface compared to open-channel flow conditions. In mid-winter conditions (Lotsari et al., 2017; Polvi et al., 2020) the high-velocity core has been observed to be lower than in open-channel conditions in the study sites of Sävar and Pulmanki Rivers. However, based on the nature of the data of this paper, we were not able to detect if the surface flow velocity influences ice advancement. This is a topic of further studies. Although we did not analyze the full 3D flow field within the cross-section, the reduction of surface flow velocities indicates that ice affects the flow velocity distribution within a cross-section. The greatest variability in velocities within the still-open part of the cross-section occurred when around 60% of the cross-section was already ice-covered.

In addition to the variation in surface flow velocities between different rivers, there was variation in the timing of frazil ice occurrences. Frazil ice formation requires two simultaneous conditions: supercooled water and turbulent flow (Beltaos, 2013). The fastest closure of the river channel took place at the Koita River, where two episodes of frazil ice were observed. At the Sävar River, frazil ice occurred continuously for seven days due to a week-long very cold period. A similar seven-day continuous period of frazil ice formation was observed at the Pulmanki River, although air temperatures were warmer and varied more during this period compared to the Sävar River. Nevertheless, the formation of frazil ice was daily and continuous. A similar case of recurring formation of frazil ice was also observed by Richard and Morse (2008). Chen et al. (2023) stated that continuous formation of frazil ice is possible. Frazil ice typically forms from the evening onwards when temperatures are cold, lasting several hours and observed over multiple days (Richard and Morse, 2008). Gosink and Osterkamp (1983) noted that frazil ice formation in the river can lead to stratification or mixing within the flow, reducing flow velocity. No clear impact of frazil ice on flow velocities was seen in this study. Although flow velocities decreased during the formation of frazil ice, this could also be attributed to the expansion of the ice cover.

Peters et al. (2018) highlighted the need to investigate the effects of asymmetric ice covers (where left and right banks have different border-ice widths) on flow characteristics beneath a partial ice cover. They also emphasized the importance of considering the effects of channel aspect and shape on flow redistribution. Our study addresses these questions based on the different channels examined. The Pulmanki River exhibited asymmetric ice cover development, with the ice cover increasing faster on the right bank side, where flow depths were shallower than on the left bank side. This asymmetry could explain the greatest variation in flow velocities within the cross-section during the freezing period when 60–80% of the channel was ice-covered. The fastest velocities occurred on the deeper left bank side. The channel cross-sectional form was most symmetrical in the Sävar River, where the decrease in velocities was steady. At the Koita River, the cross-section was the deepest and had the steepest banks, with the left bank being vertical. The ice development and break-up were the fastest in this deep, symmetrical cross-section of the Koita River. Both the Koita and Sävar Rivers had rapids a few hundred meters downstream, but this did not appear to cause similarities in ice development and break-up.

Based on air temperature measurements and long-term averages (Appendix C) during the freeze-up period, the Pulmanki River experienced colder intervals than usual. The warmest daily temperatures were at the long-term average levels, while the coldest daily temperatures were 10–19 °C colder than the average temperature. This extended period of lower air temperatures accelerated the formation of ice. At the Koita River, daily temperatures were at the long-term average level before freeze-up and dropped below the average on the day preceding the onset of freezing. At the Sävar River, air temperatures remained in line with the long-term average until November 25th, when they dropped below the average. Daily temperatures stayed entirely below the long-term average until December 9th, indicating that temperatures were colder than usual during the freezing period.

During the melting phase, similar patterns in surface velocities and ice behavior were observed across all rivers. In the Pulmanki River, the melting ice opened the channel, and when approximately 60–70% of the channel was open, flow velocities rose to near peak levels, with the highest velocities recorded when about 50% of the channel was still covered with ice. This was because the section of the channel with the highest flow observed throughout the measurement periods was then free of ice. In the Koita River, the increase in flow velocity was steady as the ice melted from the edges toward the center, with ice breaking off and flowing away. In the Sävar River, a relatively steady increase in flow velocities and ice melting was initially observed. Over one day, more than 40% of the ice broke off, significantly opening the channel. Following this, flow velocity continued to increase for another four days before decreasing. It was also observed in the Sävar River that, along with the increase in flow velocities, the discharge and water level began to rise simultaneously. Analyses from all rivers revealed how surface flow velocities increased rapidly as the ice cover opened (doi.org/10.5281/zenodo.14102870). In the Pulmanki and the Sävar rivers, the highest velocities were reached before the ice had completely melted, which could indicate that the high-velocity core had already risen close to the surface, even though ice still remained along the channel edges. Statistical analyses indicated that these three factors were strongly correlated with each other. This may have also been the cause of ice break-up in the other rivers. Increased river discharge and rising water levels, combined with rising temperatures, exert pressure on the ice cover, facilitating ice break-up (Prowse et al. 2007). As faster-flowing water beneath the ice tears it away and rising water levels bend the ice, a point is reached where the ice breaks off. Such a situation, leading to ice break-up, was observed in all the rivers. Higher flow velocity can indeed reduce ice cover, as faster-flowing water carries more thermal energy and can break up or melt the ice cover. It is possible that ice melting through other mechanisms can accelerate flow velocity as well. As mentioned in the article, the location of high-velocity core in vertical direction can vary depending on the extent of the ice and therefore the impact of its roughness, and this also alters flow velocities.

When comparing measured air temperatures with long-term averages (Appendix C), the Pulmanki River experienced a significantly warmer period before the first ice break-up, which contributed to the melting of ice and snow. During the onset of freezing, temperatures were below average; however, with daytime temperatures exceeding 0 °C, the ice began to melt. At the Koita River, temperatures were slightly warmer than the long-term average during ice break-up. In contrast, at the Sävar River, recorded temperatures were notably higher than the long-term average, facilitating the melting of snow and ice, as well as ice break-up.

The observed correlations revealed the relationships between the measured variables. Discharge and flow velocity are strongly related to each other in the river. During the freezing period, water level was unusually positively correlated with ice cover. From the images, we observed that the water level rose before freezing, even though the discharge was continuously decreasing. A bridge downstream of the study site narrows the river, may have caused a small ice dam during the freezing period, allowing the water level to rise despite the decrease in discharge and flow velocity. In spring, decreasing temperatures can influence freezing, which may facilitate freezing and simultaneously prevent water from entering the river, thereby reducing discharge and velocities. Rising temperatures in the spring can increase melting, leading to higher discharges and water levels, which can accelerate the breakup of the ice cover. However, there is no positive correlation between temperature and river discharge-related variables.

The multiple linear regression models provided further insights into these relationships. For the freezing period in the autumn, the model effectively captured the dynamics of ice cover changes. Maximum surface velocity had a significant negative impact on ice cover, while air temperature also showed a negative but smaller effect. These results highlight the dominant role of water movement in reducing ice cover during freezing periods, with temperature changes also contributing. For the thawing period in spring, the linear regression model revealed that maximum velocity had a significant negative relationship with ice cover, indicating that higher flow velocities reduce ice cover. In contrast, air temperature had a significant positive impact, suggesting that higher temperatures contribute to the formation of ice. These findings emphasize the importance of water movement in reducing ice cover during the freezing period, while temperature also plays a significant role. Additionally, the strong connection between flow velocity and discharge underscores the interdependence of these variables in influencing ice cover dynamics. Overall, these findings underscore the complex interplay between temperature, water movement, and discharge in influencing ice cover dynamics. Both correlation and regression analyses consistently show that while air temperature is a key factor, the physical forces exerted by water flow and discharge are critical in determining the extent and duration of ice cover during both freezing and thawing periods.

The data effectively demonstrated how ice development and break-up processes occur and how velocities evolve with the degree of ice coverage. Uncertainties in the data and analyses arise from the quality of the videos. For instance, the RGB cameras could not film during night-time in the autumn freezing period due to the lack of daylight, which may have caused us to miss the exact timing of the frazil ice and surface flow velocity development. The expanding ice cover also caused challenges for the velocity analysis. Water near the ice edge appeared almost stationary in some cases or turbulent in other videos, making it very difficult to determine downstream velocities. Importantly, the method requires visible movement on the water surface to function effectively. Water level errors can also impact image orthorectification and flow depth computation. If the water level is overestimated, surface velocities and wetted width may be underestimated, while flow depths are overestimated (Le Coz et al. 2021). In our study, temperature measurements were taken from a single point, both from below the water and in the air. The surface water temperature fluctuates near the ice and can affect how the ice forms. This effect could not be verified because we were unable to place temperature sensors around the river. It would have been valuable to observe whether the surface water temperature near the ice edge influenced the freezing progression. We recommend that future studies assess whether slower flow at the ice edge enables the water to cool and the ice to expand.

When calculating error values, the entire cross-section was considered. The points at the edges of the channel were the most challenging for velocity analysis due to the difficulty in detecting water movement caused by lighting conditions and stagnant water. Including these edge points also inherently increased the error values. In the comparison of reference velocities for the autumn measurements, the discrepancies were significantly larger compared to the spring measurements. During the autumn measurements on the Pulmanki River, we arrived when the largest frazil ice floes were present in the river. Conducting ADCP measurements amidst these moving frazil ice floes made data collection challenging, resulting in "patchy" data with errors, which is reflected in the reference measurement values. In the autumn, we also had to use a different instrument on the Sävar River, conducting measurements manually with an electromagnetic velocimeter. The reference velocities obtained with this data differed the most compared to all other measurements. For the spring data, the overall cross-sectional error was below 10%, which can mean a very small error for individual values.

The STIV method is one type of image velocimetry method, and it would be interesting to test different methods for the analyses. The PTV method (Eltner et al., 2021) was tried, but due to the lack of detailed camera lens information, such as focal length, the PTV analyses were not possible and were discarded from this current study. We did not have the opportunity to disassemble our cameras to define these parameters, so the PTV analyses remain to be done from the time-lapse videos of these three study sites. Particle tracking velocimetry (PTV) would have been able to detect particle motion more freely throughout the cross-section without needing to assign a pre-determined output interval. In the STIV method, the user manually sets the study line and study points, which can introduce slight directional errors. To minimize this, lines in various directions were tested and the flow direction was examined from the videos. However, in the PTV method, this error is eliminated as the software observes the direction instead of the user. The main limitations of this method are likely related to the quality of the camera. The higher the spatial resolution at which the analysis is performed, the better the quality of the analysis results. In this experiment, an easily obtainable, lower-priced durable camera was used, which performed adequately within the scope of the study. In addition to experimenting with different velocimetry methods, creating a numerical two- or three-dimensional hydrodynamic model of velocities would be highly interesting to explore. Since the data collection for this paper, additional data has been collected from the study areas using improved sensors and covering a larger area, potentially enabling more comprehensive modeling and analysis in further studies.

6. Conclusions

This study provides a description of river ice development in relation to flow velocities in three different types of cold climate rivers, during both fall freeze and spring melt periods. This paper is, to our knowledge, the first study with this extensive spatial and temporal scale, including a large time-lapse camera dataset for image velocimetry analyses. The results show variability in flow velocities and ice development between rivers, especially during the freeze-up period, which provides valuable insights for future climate change impact simulation studies. Based on the time-lapse camera datasets and their analysis with space–time image velocimetry, the following conclusions can be drawn:

1) The study revealed variations in the interaction between ice cover and flow velocities in three studied rivers. The Pulmanki River showed the most rapid decrease in flow velocity during freezing due to increased friction from the ice cover.
2) The study rivers exhibited different responses in surface flow velocities and frazil ice occurrence. Continuous frazil ice formation was observed in the Sävar and Pulmanki Rivers, while intermittent episodes were present in the Koita River.
3) Air temperature played a critical role in freezing and melting. Colder intervals accelerated freezing, while warmer temperatures during the melting phase contributed to ice break-up in all rivers.
4) Similar patterns in surface velocities and ice behavior were observed during the melting phase. The Pulmanki River had the highest flow velocities when 60–70% of the channel was open, while the Koita and Sävar Rivers showed a steady increase in flow velocities as the ice melted.
5) Regression models highlighted the complex interactions between air temperature, water movement, and ice coverage. Maximum surface flow velocity had a significant negative effect on ice cover, while air temperature also influenced ice dynamics. Flow velocity and discharge were strongly correlated, emphasizing their role in ice cover change.
6) The STIV method proved suitable for the detection of flow and ice raft velocities at different study sites. Despite the different cameras installed at different sites, and the varying quality of the GCPs (on trees at Koita River), the data could be processed with good consistency to the measured ADCP velocity data sets. Thus, the method shows potential for detecting river ice and flow development in a variety of rivers based on inexpensive time-lapse trail cameras and their videos.

Notable variations were found in the interaction between ice cover and flow velocities among the Pulmanki, Sävar, and Koita Rivers, with the Pulmanki River showing the most rapid decline in flow velocities during freezing due to increased friction from the ice cover. Rivers exhibited varied responses in surface flow velocities and frazil ice occurrences, with continuous frazil ice formation in the Sävar and Pulmanki Rivers and intermittent episodes in the Koita River. Temperature played a crucial role in freezing and melting, accelerating ice growth during colder intervals and contributing to ice break-up during warmer periods. During the melting phase, the Pulmanki River had the highest flow velocities when the channel was largely open, while the Koita and Sävar Rivers showed steady increases in flow velocities as ice melted. Regression models highlighted the interplay between air temperature and water movement showing that maximum flow velocity negatively impacted ice cover, while air temperature also influenced ice dynamics. The STIV method proved effective for detecting flow and ice rafting velocities, demonstrating its potential for monitoring river ice and flow development using inexpensive time-lapse cameras.

The results showed that with this small sample of northern rivers, located in northern Fenno-Scandinavia, we are already noticing differences in freezing cycles and impacts on river flow at the present time. Therefore, this study shows how crucial is it is to observe processes and develop measurements in various seasonally ice-covered river systems, for gaining more knowledge of changes in seasonal fluvial process magnitudes under changing climatic conditions. These will enable prediction how trends in interactions between river ice and flow characteristics will change, and what kind of impact these changes will have on the development of our rivers and habitants living next to them. These findings provide valuable insights for managing river systems in cold climates.

CRediT authorship contribution statement

T. Takala: Writing – review & editing, Writing – original draft, Visualization, Validation, Methodology, Investigation, Formal analysis, Data curation, Conceptualization. **E. Lotsari:** Writing – review & editing, Writing – original draft, Supervision, Resources, Project administration, Funding acquisition, Data curation, Conceptualization. **L.E. Polvi:** Writing – review & editing, Data curation, Conceptualization.

Declaration of competing interest

The authors declare that they have no known competing financial interests or personal relationships that could have appeared to influence the work reported in this paper.

Acknowledgements

We would like to thank for their valuable fieldwork assistance in 2020–2022 the following researchers: Dr. Anette Eltner and Dr. Melanie Elias from TU Dresden, Germany, and Dr. Erik van Rooijen from Aalto university, Finland (related to Pulmanki River in 2021 October and 2022 spring, respectively), Dr. Richard Mason from Umeå university, Sweden (related to Sävar River in 2021-22), and MSc Marko Kärkkäinen from the University of Eastern Finland, Finland (related to Koita River in autumn 2020). We also thank MSc Juha-Matti Välimäki from Aalto university, Finland, for assisting in the selection of the most suitable flow velocity tool for the analyses. The authors have no conflicts of interest to declare. The river-ice related measurements were initiated at Pulmankijoki River in 2014 under the post-doctoral research project of Dr. E. Lotsari, funded by the Research Council of Finland (ExRIVER: grant number 267345), and this paper is a continuum in the series of these winter season studies. The work for this paper was financially supported by four other projects funded by the Research Council of Finland (DefrostingRivers: 338480; HYDRO-RDI-Network: 337394; Digital Waters [DIWA] Flagship; 359248). In addition, the work was funded by The European Union – NextGenerationEU Recovery instrument (RRF) through Research Council of Finland projects Hydro RI Platform (346167) and Green-Digi-Basin (347703). Also funding was received from MVTT, Maa- ja vesitekniikan tuki ry: "Changing northern rivers and their material transport under warming climatic conditions" (grant number 43465). The Department of Geographical and Historical Studies, University of Eastern Finland, Finland, supported financially the field work done at Koita River. The work by Dr. L. E. Polvi at the Sävar River was financed by a grant (2023-01513) from the Swedish Research Council Formas, Sweden.

Appendix A. Target accuracies (in cm) at the three study sites measured with a Trimble R12i RTK-GNSS

Study site	H ave	V ave	H stdev	V stdev
Pulmanki	1.82	2.98	0.25	0.57
Sävar	2.05	3.6	0.56	1.07
Koita	2.56	4.13	1.21	1.8

Appendix B. GCP errors acquired from Hydro-STIV software from every measuring location in autumn and spring

Pulmanki River autumn 2021

ID	x(m)	y(m)	height(m)	x(pix)	y(pix)	error dx(m)	error dy(m)
No.1	7758384	539853.7	16.647	216.561	1784.073	0.131	0.033
No.2	7758384	539853.5	16.576	621.932	1782.428	0	0.015
No.3	7758383	539853.1	16.735	1037.407	1774.438	−0.137	−0.037
No.4	7758382	539898.5	15.807	728.858	288.507	0.069	−0.326
No.5	7758389	539,899	15.83	385.007	370.842	0.076	0.598
No.6	7758396	539900.1	15.521	48.244	474.682	−0.139	−0.282

Pulmanki river spring 2022

ID	x(m)	y(m)	height(m)	x(pix)	y(pix)	error dx(m)	error dy(m)
No.1	7758384	539853.7	16.647	238.814	1807.54	0.329	0.093
No.2	7758384	539853.5	16.576	645.703	1802.07	−0.017	−0.009
No.3	7758383	539853.1	16.735	1062.84	1791.84	−0.355	−0.161
No.4	7758382	539898.5	15.807	738.455	306.723	0.437	−0.318
No.5	7758389	539,899	15.83	395.108	391.619	0.096	0.58
No.6	7758396	539900.1	15.521	59.916	499.077	−0.49	−0.186

Koita River

ID	x(m)	y(m)	height(m)	x(pix)	y(pix)	error dx(m)	error dy(m)
No.1	7758384	539853.7	16.647	238.814	1807.54	0.329	0.093
No.2	7758384	539853.5	16.576	645.703	1802.07	−0.017	−0.009
No.3	7758383	539853.1	16.735	1062.84	1791.84	−0.355	−0.161
No.4	7758382	539898.5	15.807	738.455	306.723	0.437	−0.318
No.5	7758389	539,899	15.83	395.108	391.619	0.096	0.58
No.6	7758396	539900.1	15.521	59.916	499.077	−0.49	−0.186

Sävar River autumn 2021

ID	x(m)	y(m)	height(m)	x(pix)	y(pix)	error dx(m)	error dy(m)
metarg4	7125941	760304	112.553	322.877	1709.443	0.154	−0.298
metarg5	7125940	760304.7	112.456	812.384	1684.26	−0.167	0.296
wootarg1	7125964	760312.5	112.445	490.122	63.715	−0.438	−0.173
wootarg2	7125963	760314.8	112.394	730.548	36.137	0.019	0.011
wootarg3	7125962	760317.4	112.23	991.853	26.896	−0.145	−0.028
metarg1	7125964	760312.7	112.015	512.4	91.858	0.216	0.048
metarg2	7125963	760313.7	111.971	618.975	87.834	0.191	0.06
metarg3	7125963	760314.5	112.001	704.22	76.926	0.169	0.085

Sävar River spring 2022

ID	x(m)	y(m)	height(m)	x(pix)	y(pix)	error dx(m)	error dy(m)
metarg4	7125941	760304	112.553	317.014	1884.467	0.257	−0.738
metarg5	7125940	760304.7	112.456	821.273	1844.049	−0.309	0.715
wootarg1	7125964	760312.5	112.445	472.481	230.797	−0.546	0.153
wootarg2	7125963	760314.8	112.394	704.876	204.967	−0.01	−0.129
wootarg3	7125962	760317.4	112.23	956.046	200.699	0.094	−0.598
metarg1	7125964	760312.7	112.015	494.557	257.207	0.027	0.322
metarg2	7125963	760313.7	111.971	598.402	252.727	0.214	0.193
metarg3	7125963	760314.5	112.001	681.953	242.738	0.273	0.081

Appendix 3. Long range average air temperatures plotted with the temperatures during the measurement times. Temperatures from A Pulmanki River, B Koita River and C Sävar river

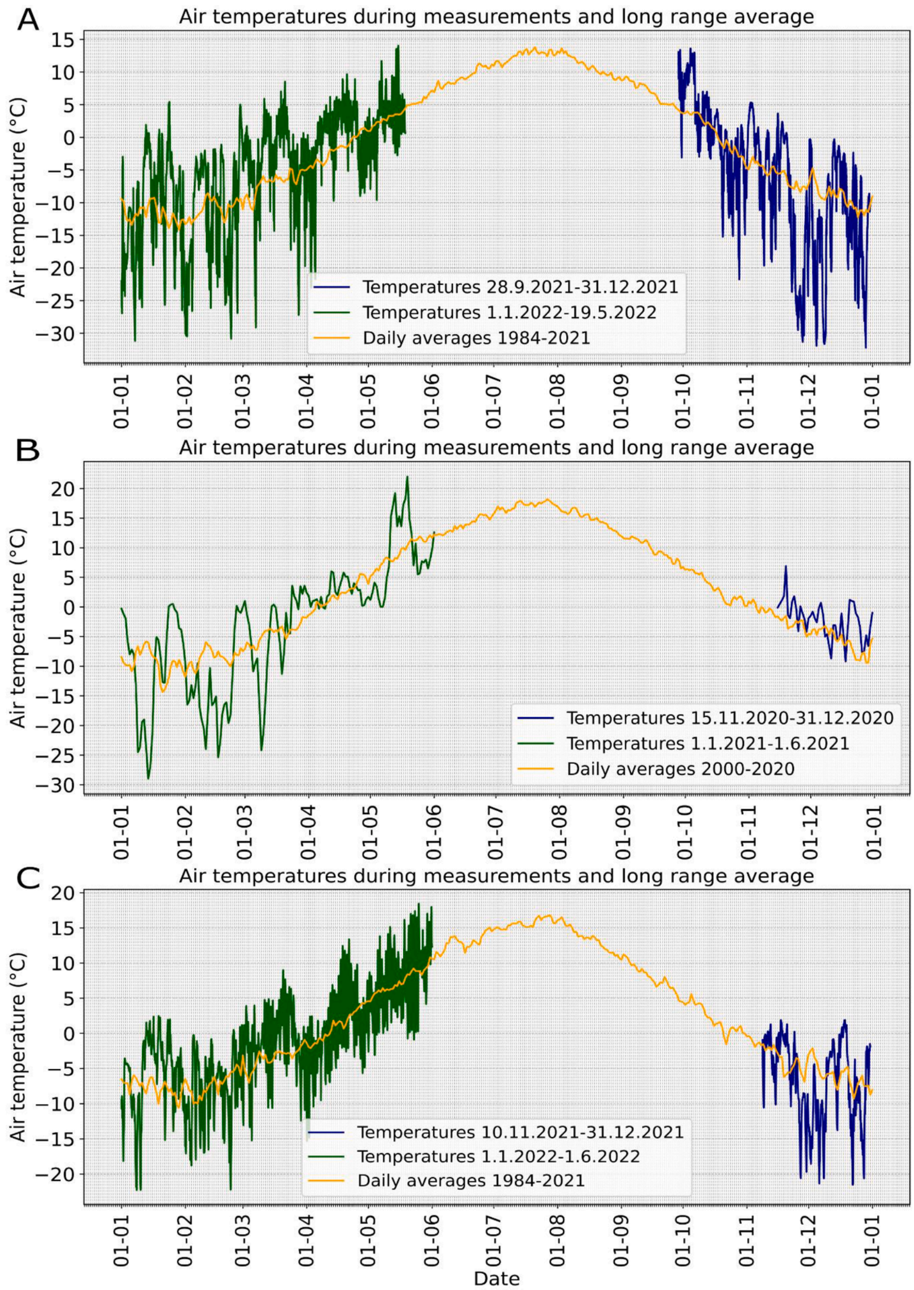

References

Adrian, R.J., 1984. Scattering particle characteristics and their effect on pulsed laser measurements of fluid flow: speckle velocimetry vs particle image velocimetry. In: Applied Optics, vol. 23. Optica Publishing Group, p. 1690. https://doi.org/10.1364/ao.23.00169, 11.

Adrian, R.J., 2005. Twenty years of particle image velocimetry. Experiments in Fluids 39, 159–169. https://doi.org/10.1007/s00348-005-0991-7.

AMAP, 2011. Snow, Water, Ice and Permafrost in the Arctic (SWIPA): Climate Change and the Cryosphere. Arctic Monitoring and Assessment Programme (AMAP), Oslo, Norway. xii + 538 pp.

Andréasson, J., Bergström, S., Carlsson, B., Graham, L.P., Lindström, G., 2004. Hydrological change – climate Change Impact Simulations for Sweden. Ambio 33, 228–234. https://doi.org/10.1579/0044-7447-33.4.228.

Beltaos, S., 2013. *River ice formation*. Committee on river ice processes and the environment, Canadian geophysical union hydrology section.

Carstens, T., 1966. Experiments with supercooling and ice formation in flowing water. Geofysiske Publikasjoner 26, 1–18.

Casson, N.J., Eimers, M.C., Watmough, S.A., 2012. Impact of winter warming on the timing of nutrient export from forested catchments. Hydrol. Processes 26, 2546–2554. https://doi.org/10.1002/hyp.8461.

Chen, Y., Lian, J., Zhao, X., Guo, Q., Yang, D., 2023. Advances in Frazil ice evolution mechanisms and numerical modelling in rivers and channels in Cold Regions. Water 15 (14), 2582. https://doi.org/10.3390/w15142582.

Clark, S.P., Doering, J.C., 2009. Frazil flocculation and secondary nucleation in a counterrotating flume. Cold Regions Sci. Technol. 55, 221–229. https://doi.org/10.1016/j. coldregions.2008.04.002.

Daly, S.F., Crrel (U.S.), 1984. Frazil ice Dynamics. US Army Corps of Engineers, Cold Regions Research & Engineering Laboratory.

Demers, S., Buffin-Bélanger, T., Roy, A.G., 2011. Helical cell motions in a small ice-covered meander river reach. River Res. Appl. 27, 1118–1125. https://doi.org/10.1002/rra.1451.

Demers, S., Buffin-Bélanger, T., Roy, A.G., 2012. Macroturbulent coherent structures in an ice-covered river flow using a pulse-coherent acoustic Doppler profiler. Earth Surf. Processes Landforms 38 (9), 937–946. https://doi.org/10.1002/esp.3334. Wiley.

Eltner, A., Bertalan, L., Grundmann, J., Perks, M.T., Lotsari, E., 2021. Hydro-morphological mapping of river reaches using videos captured with unoccupied aerial systems. Earth Surf. Processes Landforms 46, 2773–2787. https://doi.org/10.1002/esp.5205.

Fujita, I., Watanabe, H., Tsubaki, R., 2007. Development of a non-intrusive and efficient flow monitoring technique: the space-time image velocimetry (STIV). Int. J. River Basin Manage. 5 (2), 105–114. https://doi.org/10.1080/15715124.2007.9635310.

Fukś, M., 2023. Changes in river ice cover in the context of climate change and dam impacts: a review. Aquatic Sci. 85, 113. https://doi.org/10.1007/s00027-023-01011-4.

Gosink, J.P., Osterkamp, T.E., 1983. Measurements and analyses of velocity profiles and frazil ice crystal rise velocities during periods of frazil-ice formation in rivers. Ann. Glaciol. 4, 79–84. https://doi.org/10.3189/S0260305500005279.

Hirvas, H., Lagerbäck, R., Mäkinen, K., Nenonen, K., Olsen, L., Rodhe, L., Thoresen, M., 1988. The Nordkalott project: studies of quaternary geology in northern Fennoscandia. Boreas 17 (4), 431–437. https://doi.org/10.1111/j.1502-3885.1988.tb00560.x.

Hydro Technology Institute co., L., 2022. Hydro-STIV Operation Manual (Ver 1.2.2).

Ionita, M., Badaluta, C.A., Scholz, P., Chelcea, S., 2018. Vanishing river ice cover in the lower part of the Danube basin – signs of a changing climate. Nat. Scientific Rep. 8, 7948. https://doi.org/10.1038/s41598-018-26357-w.

Kämäri, M., Alho, P., Colpaert, A., Lotsari, E., 2017. Spatial variation of river-ice thickness in a meandering river. Cold Regions Sci. Technol. 137, 17–29. https://doi.org/10.1016/j.coldregions.2017.01.009. Elsevier BV.

Kämäri, M., Alho, P., Veijalainen, N., Aaltonen, J., Huokuna, M., Lotsari, E., 2015. River ice cover influence on sediment transportation at present and under projected hydroclimatic conditions. Hydrol. Processes 29 (22), 4738–4755. https://doi.org/10.1002/hyp.10522. Wiley.

Kärkkäinen, M., Lotsari, E., 2022. Impacts of rising, peak and receding phases of discharge events on erosion potential of a boreal meandering river. Hydrol. Processes 36 (10). https://doi.org/10.1002/hyp.14674.

Kasvi, E., Vaaja, M., Alho, P., Hyyppä, H., Hyyppä, J., Kaartinen, H., Kukko, A., 2012. Morphological changes on meander point bars associated with flow structure at different discharges. Earth Surf. Processes Landforms 38 (6), 577–590. https://doi.org/10.1002/esp.3303. Wiley.

Kasvi, E., Vaaja, M., Kaartinen, H., Kukko, A., Jaakkola, A., Flener, C., Hyyppä, H., Hyyppä, J., Alho, P., 2015. Sub-bend scale flow–sediment interaction of meander bends—a combined approach of field observations, close-range remote sensing and computational modelling. Geomorphology 238, 119–134. https://doi.org/10.1016/j.geomorph.2015.01.039. Elsevier BV.

Le Coz, J., Renard, B., Vansuyt, V., Jodeau, M., Hauet, A., 2021. Estimating the uncertainty of video-based flow velocity and discharge measurements due to the conversion of field to image coordinates. Hydrol. Processes 35 (5). https://doi.org/10.1002/hyp.14169. Wiley.

Lind, L., Nilsson, C., 2015. Vegetation patterns in small boreal streams relate to ice and winter floods. J. Ecol. 103, 431–440. https://doi.org/10.1111/1365-2745.12355.

Lotsari, E., Kasvi, E., Kämäri, M., Alho, P., 2017. The effects of ice-cover on flow characteristics in a subarctic meandering river. Earth Surf. Processes Landforms 42, 1195–1212. https://doi.org/10.1002/esp.4089.

Lotsari, E., Lind, L., Kämäri, M., 2019. Impacts of hydro-climatically varying years on ice growth and decay in a subarctic river. Water 11 (10), 2058. https://doi.org/10.3390/w11102058. MDPI AG.

Lotsari, E., Dietze, M., Kämäri, M., Alho, P., Kasvi, E., 2020. Macro-turbulent flow and its impacts on sediment transport potential of a subarctic river during ice-covered and open-channel conditions. Water 12 (7), 1874. https://doi.org/10.3390/w12071874. MDPI AG.

MacDonald, M.K., Stadnyk, T.A., Déry, S.J., Braun, M., Gustafsson, D., Isberg, K., Arheimer, B., 2018. Impacts of 1.5 and 2.0 °C warming on pan-Arctic river discharge into the Hudson Bay Complex through 2070. Geophys. Res. Lett. 45, 7561–7570. https://doi.org/10.1029/2018GL079147.

Magnuson, J.J., Robertson, D.M., Benson, B.J., Wynne, R.H., Livingstone, D.M., Arai, T., Assel, R.A., Barry, R.G., Card, V., Kuusisto, E., Granin, N.G., Prowse, T.D., Stewart, K. M., Vuglinski, V.S., 2000. Historical trends in lake and river ice cover in the Northern Hemisphere. Science 289, 1743–1746. https://doi.org/10.1126/science.289.5485.1743.

McFarlane, V., Loewen, M., Hicks, F., 2015. Measurements of the evolution of frazil ice particle size distributions. Cold Regions Sci. Technol. 120, 45–55. https://doi.org/10.1016/j.coldregions.2015.09.001.

McFarlane, V., Loewen, M.R., Hicks, F., 2017. Measurements of the size distribution of frazil ice particles in three Alberta rivers. Cold Regions Sci. Technol. 142, 100–117. https://doi.org/10.1016/j.coldregions.2017.08.001.

Metsähallitus, 2006. Koitajoen Natura-alueen hoito-ja käyttösuunnitelma. Metsähallituksen luonnonsuojelujulkaisuja, Sarja C4.

Michel, B., Marcotte, N., Fonseca, F., Rivard, G., 1982. Formation of border ice in the Ste-Anne River. In: 2nd Workshop on Hydraulics of Ice Covered Rivers, Edmonton, Canada. pp. 38–61.

Murray, A., Essel, E., Dow, K., 2022. Particle image velocimetry investigation of void seepage through a simulated ice jam. Cold Regions Sci. Technol. 196, 103493. https://doi.org/10.1016/j.coldregions.2022.103493.

Norrgård, S., Helama, S., 2022. Tricentennial trends in spring ice break-ups on three rivers in northern Europe. Cryosphere 16, 2881–2898. https://doi.org/10.5194/tc-16-2881-2022.

Nyantekyi-Kwakye, B., Essel, E.E., Dow, K., Clark, S.P., Tachie, M.F., 2020. Hydraulic and turbulent flow characteristics beneath a simulated partial ice-cover. J. Hydraulic Res. 59 (3), 392–403. https://doi.org/10.1080/00221686.2020.1780493. Informa UK Limited.

Peel, M.C., Finlayson, B.L., McMahon, T.A., 2007. Updated world map of the Köppen-Geiger climate classification. Hydrol. Earth Syst. Sci. 11 (5), 1633–1644. https://doi.org/10.5194/hess-11-1633-2007. Copernicus GmbH.

Peters, M., Dow, K., Clark, S.P., Malenchak, J., Danielson, D., 2017. Experimental investigation of the flow characteristics beneath partial ice covers. Cold Regions Sci. Technol. 142, 69–78. https://doi.org/10.1016/j.coldregions.2017.07.007. Elsevier BV.

Peters, M., Clark, S.P., Dow, K., Malenchak, J., Danielson, D., 2018. Flow characteristics beneath a simulated partial ice cover: effects of ice and bed roughness. J. Cold Regions Eng. 32 (1). https://doi.org/10.1061/(asce)cr.1943-5495.0000143.

Polvi, L.E., Dietze, M., Lotsari, E., Turowski, J.M., Lind, L., 2020. Seismic monitoring of a subarctic river: seasonal variations in hydraulics, sediment transport, and ice dynamics. J. Geophys. Res.: Earth Sur. 125 (7), 5. https://doi.org/10.1029/2019jf005333. American Geophysical Union (AGU).

Prowse, T.D., 2001. River-ice ecology. I: hydrologic, geomorphic, and water-quality aspects. J. Cold Regions Eng. 15, 1–16. https://doi.org/10.1061/(ASCE)0887-381X(2001)15:1(1).

Prowse, T.D., 2001b. River-ice ecology. II: biological aspects. J. Cold Regions Eng. 15 (1), 17–33. https://doi.org/10.1061/(asce)0887-381x(2001)15:1(17). American Society of Civil Engineers (ASCE).

Prowse, T.D., Bonsal, B.R., Duguay, C.R., Lacroix, M.P., 2007. River-ice break-up/freeze-up: a review of climatic drivers, historical trends and future predictions. Ann. Glaciol. 46, 443–451. https://doi.org/10.3189/172756407782871431.

Prowse, T.D., 2005. River-ice hydrology. In: Encyclopedia of Hydrological Sciences, edited by: Anderson, M. G., John Wiley and Sons Ltd., West Sussex, England, 2657–2677. DOI:10.1002/0470848944.HSA177.

Richard, M., Morse, B., 2008. Multiple frazil ice blockages at a water intake in the St. Lawrence River. Cold Regions Sci. Technol. 53 (2), 131–149. https://doi.org/10.1016/j.coldregions.2007.10.003. Elsevier BV.

Rohacs, D., Yasar, O., Kale, U., Ekici, S., Yalcin, E., Midilli, A., Karakoc, T.H. 2023. Past and current components-based detailing of particle image velocimetry: a comprehensive review. https://doi.org/10.1016/j.heliyon.2023.e14404.

Rouzegar, M., Clark, S.P., 2023. Experimental investigation of sediment transport in partially ice-covered channels. Int. J. Sedim. Res. 38 (5), 769–779. https://doi.org/10.1016/j.ijsrc.2023.06.003. Elsevier BV.

Swedish Meteorological and Hydrological Institute, 2023. Open data – Ladda ner hydrologiska observationer, Vattenföring (15 min), YTTERTRÄSK NEDRE. <https://www.smhi.se/data/hydrologi/ladda-ner-hydrologiska-observationer#param=waterdischarge15min,stations=core,stationid=2236>.

Swedish Meteorological and Hydrological Institute, 2024. SMHIs vattenföringsmätningar. 6.11.2024. <https://www.smhi.se/kunskapsbanken/hydrologi/matning-av-flode-och-vattenstand/smhis-vattenforingsmatningar-1.80833>.

Thellman, A., Jankowski, K.J., Hayden, B., Yang, X., Dolan, W., Smits, A.P., O'Sullivan, A.M., 2021. The ecology of river ice. J. Geophys. Res. Biogeosci. 126, e2021JG006275. https://doi.org/10.1029/2021JG006275.

Veijalainen, N., Lotsari, E., Alho, P., Vehviläinen, B., Käyhkö, J., 2010. National scale assessment of climate change impacts on flooding in Finland. J. Hydrol. 391, 333–350.

Watanabe, K., Fujita, I., Iguchi, M., Hasegawa, M., 2021. Improving accuracy and robustness of space-time image velocimetry (STIV) with deep learning. Water 13 (15), 2079. https://doi.org/10.3390/w13152079. MDPI AG.

Wolff, F., Lorenz, S., Korpelainen, P., Eltner, A., Kumpula, T., 2024. UAV and field hyperspectral imaging for Sphagnum discrimination and vegetation modelling in Finnish aapa mires. Int. J. Appl. Earth Obs. Geoinf. 134, 104201. https://doi.org/10.1016/j.jag.2024.104201. Elsevier BV.

Yang, X., Pavelsky, T.M., Allen, G.H., 2020. The past and future of global river ice. Nature 577 (7788), 69–73. https://doi.org/10.1038/s41586-019-1848-1.

Yeh, M.-T., Chung, Y.-N., Huang, Y.-X., Lai, C.-W., Juang, D.-J., 2019. Applying adaptive LS-PIV with dynamically adjusting detection region approach on the surface velocity measurement of river flow. Comput. Electr. Eng. 74, 466–482. https://doi.org/10.1016/j.compeleceng.2017.12.013.

Zhao, H., Chen, H., Liu, B., Liu, W., Xu, C.-Y., Guo, S., Wang, J., 2021. An improvement of the Space-Time Image Velocimetry combined with a new denoising method for estimating river discharge. Flow Meas. Instrum. 77, 101864. https://doi.org/10.1016/j.flowmeasinst.2020.101864. Elsevier BV.